AD

USAAVLABS TECHNICAL REPORT 68-45

AN EXPERIMENTAL INVESTIGATION OF GROUND EFFECT ON A FOUR-PROPELLER TILT-WING V/STOL MODEL

By

William F. Putman

July 1968

U. S. ARMY AVIATION MATERIEL LABORATORIES
FORT EUSTIS, VIRGINIA

CONTRACT DA 44-177-AMC-8(T)
PRINCETON UNIVERSITY
PRINCETON, NEW JERSEY

Disclaimers

The findings in this report are not to be construed as an official Department of the Army position unless so designated by other authorized documents.

When Government drawings, specifications, or other data are used for any purpose other than in connection with a definitely related Government procurement operation, the United States Government thereby incurs no responsibility nor any obligation whatsoever; and the fact that the said drawings, specifications, or other data is not to be regarded by implication or otherwise as in any manner licensing the holder or any other person or corporation, or conveying any rights or permission, to manufacture, use, or sell any patented invention that may in any way be related thereto.

Disposition Instructions

Destroy this report when no longer needed. Do not return it to originator.

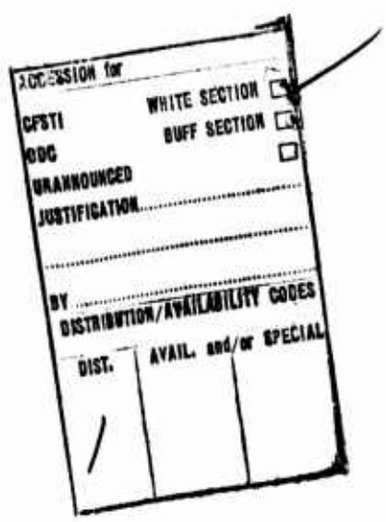

DEPARTMENT OF THE ARMY
U. S. ARMY AVIATION MATERIEL LABORATORIES
FORT EUSTIS, VIRGINIA 23604

This report has been reviewed by the U. S. Army Aviation Materiel Laboratories, the Naval Air Systems Command, and the Air Force Flight Dynamics Laboratories. It is considered to be technically sound.

This work, which was performed under Contract DA 44-177-AMC-8(T), was undertaken to determine experimentally the measurement of lift, drag, and pitching moment of a four-propeller tilt-wing V/STOL transport model on the Princeton Dynamic Model Track at various flight conditions above the ground. Experimental tests both at constant altitude and for slowly decreasing altitudes were accomplished. The ground effect phenomena based on the various flight conditions were briefly analyzed, and general data trends for these conditions were obtained. The floor under the model was tufted, and movies of the flow patterns were taken during all of these tests.

This report is published for the exchange of information and the stimulation of ideas.

Task 1F125901A14233
Contract DA 44-177-AMC-8(T)
USAAVLABS Technical Report 68-45
July 1968

AN EXPERIMENTAL INVESTIGATION OF GROUND EFFECT ON A FOUR-PROPELLER TILT-WING V/STOL MODEL

Final Report

Department of Aerospace and Mechanical Sciences
Report 892

By

William F. Putman

Prepared by

Princeton University
Princeton, New Jersey

for

U. S. ARMY AVIATION MATERIEL LABORATORIES
FORT EUSTIS, VIRGINIA

SUMMARY

Tests were conducted on a one-tenth scale model of a tilt-wing V/STOL transport at specified points simulating STOL flight conditions at various heights above the ground. The model was moved at selected velocities through still air in the Princeton Dynamic Model Track; and lift, drag, and pitching moment were measured at various heights above the ground. In addition, motion picture observations were made of the flow field adjacent to the ground by means of cameras moving with the model and photographing the motion of wool tufts attached to the floor along the entire length of the test section.

The six test conditions investigated included selected combinations of 30°, 40°, and 60° wing incidence angle with 30°, 40°, and 60° flap deflection, and values of propeller thrust coefficient based on slipstream dynamic pressure, C_{T_s}, ranging from 0.80 to 0.95. Model ground clearances of 3.5 to 36 inches were investigated both at constant altitude and with the altitude continuously varying during the run.

The data are presented as plots of lift, drag, and pitching moment coefficients based on slipstream velocity. Also included are data from wind tunnel tests on similar models.

A brief analysis is made of ground effect phenomena in the flight regime of interest, and an understanding of the general data trends is thereby obtained. The magnitude and direction of the force change in ground effect are predictable. However, the pitching moment change is strongly influenced by factors such as the flow field beneath the fuselage, the change in downwash at the horizontal tail, and other effects that are not accounted for in this report.

FOREWORD

This research was performed by the Department of Aerospace and Mechanical Sciences, Princeton University, under the sponsorship of the United States Army Aviation Materiel Laboratories Contract DA 44-177-AMC-8(T), with financial support from the United States Naval Air Systems Command and the United States Air Force Flight Dynamics Laboratory. The research was monitored by Mr. Richard L. Scharpf and Mr. Robert P. Smith of the United States Army Aviation Materiel Laboratories.

The research was conducted under the direction of Associate Professor H. C. Curtiss, Jr., of Princeton University. Mr. J. J. Traybar of Princeton University assisted in this research endeavor.

BLANK PAGE

TABLE OF CONTENTS

LIST OF ILLUSTRATIONS

LIST OF SYMBOLS

A	propeller disc area, ft^2 (1.89 ft^2)
A_m	momentum area of model, ft^2 (Reference 7)
a	lift curve slope of propeller blade element, per rad (5.75)
a.c.	aerodynamic center of wing (assumed to be at 0.25 MAC)
b	wing span, ft (6.75 ft)
$C_{D,_s}$	drag coefficient based on slipstream dynamic pressure, $\frac{D}{q_{ss} S}$
$C_{F,_s}$	resultant aerodynamic force coefficient based on slipstream dynamic pressure, $\frac{F}{q_{ss} S}$
$C_{L,_s}$	lift coefficient based on slipstream dynamic pressure, $\frac{L}{q_{ss} S}$
$C_{M,_s}$	pitching moment coefficient based on slipstream dynamic pressure, $\frac{M}{q_{ss} S\bar{c}}$
$C_{M,_{s_{CALC}}}$	pitching moment coefficient based on slipstream dynamic pressure, calculated from wing and propeller forces, $\frac{\ell_W}{\bar{c}} C_{W,_s} - \frac{\ell_T}{\bar{c}} C_{TS,_s}$
C_T	propeller thrust coefficient based on propeller disc area and tip speed, $\frac{T}{\rho A (\Omega R)^2}$
$C_{T,_s}$	propeller thrust coefficient based on propeller disc area and slipstream dynamic pressure, $\frac{T}{q_{ss} A}$
$C_{TS,_s}$	propeller thrust coefficient based on wing area and slipstream dynamic pressure, $\frac{T}{q_{ss} S}$

$C_{W,_S}$	wing resultant force coefficient, based on slipstream dynamic pressure, $\frac{F_W}{q_{ss} S}$
$C_{W,_{S_{CORR}}}$	wing resultant force corrected for ground effect
c	propeller blade chord, ft
$\bar{c}$	mean aerodynamic chord of wing, ft (0.807 ft)
cg	center of gravity and moment reference point
d	distance of propeller from 0.25 $\bar{c}$ point of wing, ft
D	drag force, lb
F	resultant aerodynamic force produced by aircraft, lb
F.S.	fuselage station, in.
F_W	resultant aerodynamic force produced by wing, lb
h	height of 0.25 MAC above ground, ft
h_b	height of fuselage bottom above ground, ft or in.
IGE	in ground effect
i_t	horizontal tail incidence, deg
i_W	wing incidence, deg
L	lift force, lb
L_W	component of wing force perpendicular to chord, lb
ℓ_M	pitching moment coefficient, expressed per unit $\bar{c}$, $\frac{C_{M,_S}}{C_{L,_S}}$
$\ell_{M;CALC}$	pitching moment coefficient, expressed per unit $\bar{c}$, calculated, $\frac{C_{M,_{S_{CALC}}}}{C_{L,_S}}$
ℓ_T	perpendicular distance of thrust axis from moment center, ft

ℓ_w	perpendicular distance of line of action of wing force from moment center, ft
LTV	Ling-Temco Vought Aerospace Corporation
M	pitching moment about moment center, positive nose up, ft-lb
MAC	mean aerodynamic chord ($\bar{c}$)
N	number of blades per propeller (4)
OGE	out of ground effect
q_∞	free-stream dynamic pressure, lb/ft^2, $\frac{1}{2} \rho V_o^2$
q_{ss}	slipstream dynamic pressure, lb/ft^2, $q_\infty + \frac{T}{A}$
R	propeller radius, ft (0.875 ft)
r	propeller radial station, ft
S	wing area, ft^2 (5.34 ft^2)
T	thrust of one propeller, lb
t	propeller blade thickness, ft
δu	horizontal influence velocity due to image vortex system, ft/sec
V_o	free-stream velocity, ft/sec
V	corrected free-stream velocity at propeller plane, ft/sec
V_{R_o}	resultant velocity at wing aerodynamic center (vector sum of free-stream velocity, propeller induced velocity, and velocity induced by wing trailing vortex system), ft/sec
V_R	corrected resultant velocity at wing aerodynamic center, ft/sec
V_{R_f}	slipstream velocity, resultant of free-stream velocity and propeller induced velocity, ft/sec
v_o	axial induced velocity at propeller plane, ft/sec
Δv	correction to propeller induced velocity, ft/sec
W.L.	waterline distance, in.
Δw	velocity induced by wing vortex system, ft/sec

δw	vertical influence velocity due to image vortex system, ft/sec
$\frac{x}{\bar{c}}$	nondimensional horizontal distance from moment center
$\frac{z}{\bar{c}}$	nondimensional vertical distance from moment center
α_{FUS}	fuselage angle of attack, deg
α_p	propeller remote angle of attack, deg, $i_w + \alpha_{FUS} - 90°$
$\Delta\alpha_p$	correction to propeller angle of attack due to presence of wing flow field, deg
β	propeller blade twist, deg
$\beta_{.75R}$	propeller blade angle at 3/4 rad, deg
β_e	effective propeller blade angle at 3/4 rad, deg
Γ	circulation around line vortex, ft^2/sec
δ_f	flap deflection, deg
$\delta_{u,D}$, $\delta_{u,L}$, $\delta_{w,D}$, $\delta_{w,L}$	nondimensional interference velocities
θ	angle between horizontal and resultant velocity at wing aerodynamic center, deg
θ_n	wake deflection angle, measured from horizontal, deg
λ	inflow ratio, $\frac{V \sin \alpha_p - V_o}{\Omega R}$
μ	advance ratio, $\frac{V}{\Omega R}$
ρ	air density, $slug/ft^3$
σ	propeller blade solidity, $\frac{N\int_o^R cdr}{\pi R^2}$
Ω	propeller rotational velocity, rad/sec unless noted

$( )'$	in ground effect
$( )_o$	initial or uncorrected value
$(\bar{})$	vector
$( )_{BV}$	contribution of bound vortex
$( )_{TV}$	contribution of trailing vortex

INTRODUCTION

Considerable interest has been shown in the prediction of force and moment variations associated with the operation of V/STOL-type vehicles during takeoff, approach, and landing manuevers that are complicated by so-called "ground effect" phenomena. Ground effect studies have become especially significant since various wind tunnel tests of models of tilt-wing V/STOL transports have indicated that the consequences of these effects may be very severe, with attendant lift losses greater than 35 percent of gross weight and a pitching moment change equivalent to a 5-percent MAC cg shift.[9,10]

However, there was reason to suspect that wind tunnel data in this particular flight regime might be inaccurate due to the boundary layer on the ground plane and/or the difficulty of measuring and maintaining constant low test section velocities. Accordingly, a program was formulated for retesting selected wind tunnel data points in the Dynamic Model Track, where the boundary conditions for the simulation of ground proximity are more correct and the velocity control is precise.

To facilitate interpretation of the experimental observations, analytical techniques were used to predict at least the trends of the data. This study also made possible recommendations for more comprehensive analytical and experimental studies aimed at developing techniques for the accurate prediction of ground effect phenomena in the V/STOL flight regime.

APPARATUS AND PROCEDURE

The model used in the subject experiments is the identical one used in the dynamic stability experiments described in Reference 1, with the addition of scaled wing leading edge slats. A photograph of the model installed on the ground proximity mount in the Dynamic Model Track is shown in Figure 1.

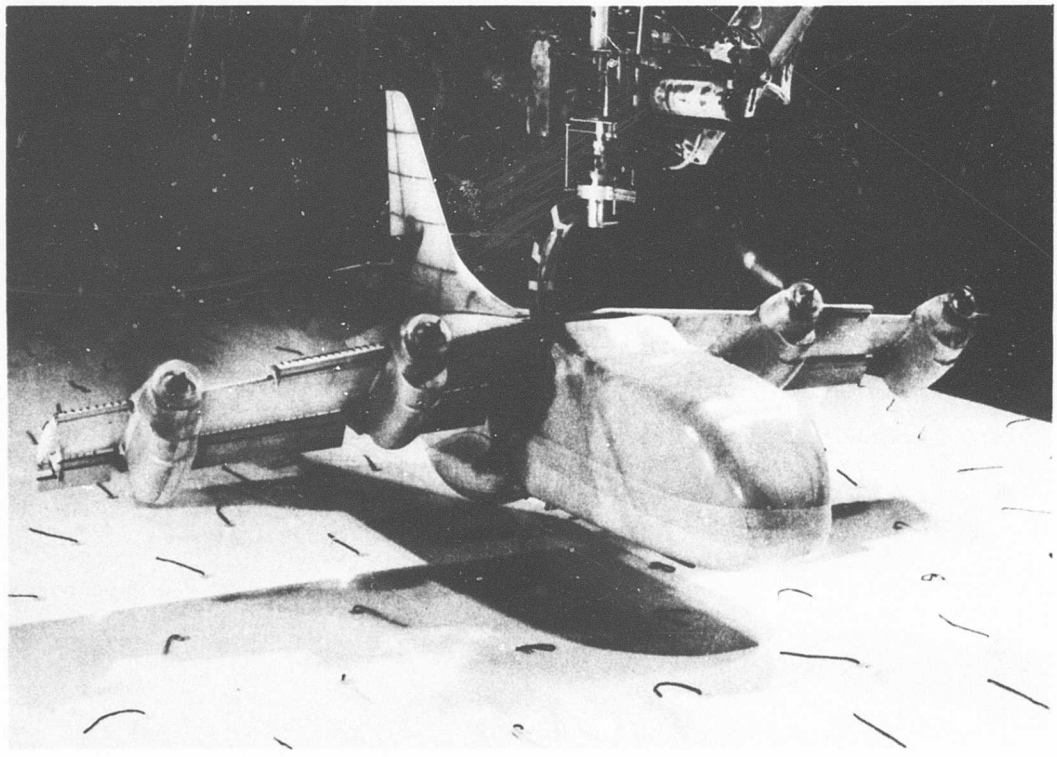

Figure 1. One-Tenth Scale Model Mounted on Test Apparatus.

The Princeton Dynamic Model Track, as described in Reference 2, was designed primarily for dynamic testing of V/STOL aircraft and helicopters. However, it possesses the unique capability of performing static testing (i.e., force and moment measuring as opposed to dynamic response) at low velocities under precisely controlled conditions. In particular, the simulation of aircraft flight in ground effect is exact in that the model is moved through still air over a still ground plane. Thus, simulation errors due to free-stream velocity gradients that might be present in wind tunnel type testing of ground effect phenomena are minimized or eliminated.

For the tests conducted, the model mount was modified to allow the model to be suspended from above, and the mounting boom was altered to allow the model to be positioned near the floor. The model could be driven at a slow vertical velocity (2 inches per second) through an altitude range of approximately 60 inches during a test run, or it could be set at a constant altitude. The former method of testing is referred to as quasi-steady-state testing. The variation of forces and moments with ground height through a selected range of heights is measured during one run using the quasi-steady-state technique. The vertical velocity is set at a value small enough that it should not influence the data. In order to verify that this effect is negligible, selected constant altitude runs were also made and are presented along with the altitude varying runs.

The Dynamic Model Track main carriage drive has a high bandwidth, high accuracy velocity servo that allows the carriage (and model) to be driven at a commanded horizontal velocity with variations in speed of less than ± 1 percent.

A typical test procedure is as follows:

> After the model and carriage controls have been set for the desired test condition, the propellers are brought up to speed. The carriage and the model are accelerated to the selected forward velocity, and the data portion of the run commences. If a variable-altitude run has been programmed, the variation in altitude commences at a particular location along the track.

A selected smooth portion (approximately 200 feet long) of the 750-foot-long track floor was used for the constant-altitude runs. No influence of floor irregularity was observable in the data.

A schematic drawing showing the test variables and the measurement axis is presented in Figure 2.

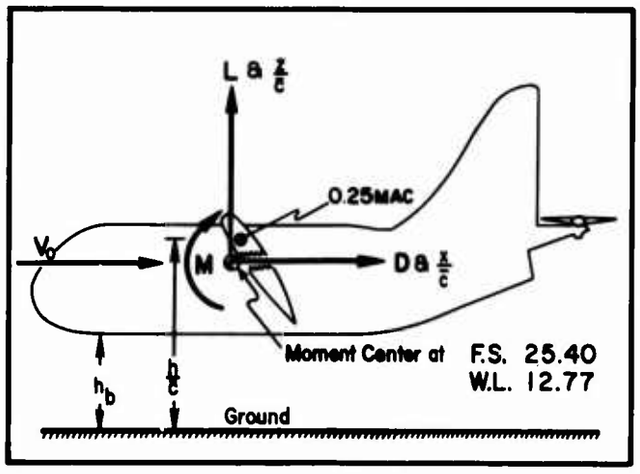

Figure 2. Axis System and Test Variables.

MODEL

A three-view drawing of the model used during the experiments is shown in Figure 3. Details of the wing section and high lift devices are given in Figure 4 (a and b). The model is dynamically similar to the LTV XC-142A.

The fuselage is constructed of an inner and outer Fiberglas skin, vacuum molded and bonded to a Styrofoam core. An aluminum box spar is the main structural member of the wing. Mahogany ribs and a vacuum-molded Fiberglas wing surface form the external airfoil shape. The double-slotted flaps are constructed of low-density Styrofoam with a Fiberglas covering.

The model drive motor is a 200-volt, 400-cycle, 3-phase electric motor, rated at 5 horsepower, mounted on a bulkhead in the fuselage. Power for the four propellers is transmitted to a central transmission and from thence to right-angle gearboxes located in the wing by flexible shafting. A separate power takeoff (which was disconnected for the present experiments) is used to drive the tail rotor. Propeller gearboxes and housings are mounted directly on the wing spar. The propeller blades were constructed of Fiberglas. The geometric characteristics of the propellers are shown in Figure 4c.

Model control positions are set from a control console on the carriage. The model incorporates electrically controllable blade angles on each of the four propellers. The blade angle of the tail rotor is also variable to provide pitching moment trim. Wing incidence, flaps, ailerons, and the horizontal tail are also power operated so that transition runs can be made with selected programming of all required controls. All of these systems are closed-loop position controls.

INSTRUMENTATION

All test data were measured at a time-sharing rate of 40 samples per second, telemetered from the moving carriage, and recorded on a magnetic tape recorder located in the test control room. A complete description of the 45-channel pulse duration modulation (PDM) telemetering and data recording system is given in Reference 2.

The force measuring instrumentation consisted of mass-balanced strain-gauge load cells adapted to the model mount normally used for dynamic tests and described in Reference 2. The mass-balancing feature eliminated acceleration inputs in these measurements; these disturbances are a common problem in any moving-model test apparatus, and in the Dynamic Model Track they arise from vibration inputs due to small irregularities in track alignment. The successful attenuation of inertial inputs to the model was greatly aided by the use of a light model, originally designed and used for dynamic stability tests.

Two independent measurements of altitude were recorded: one of the model support boom relative to the carriage and the other of the model relative

to the floor. The latter was desirable because of the slight floor irregularities and because the relative freedom between the model and carriage provided for the attenuation of acceleration inputs. The direct altitude sensing was accomplished by means of a very light, preloaded "whisker" suspended from the model and touching the floor. Tare runs were made to establish that this arrangement produced no measurable effect on the force and moment measurements.

Propeller speed was continuously measured by a DC tachometer geared to the interconnected propellers, and initial propeller rpm was determined by a "Strobotach" at the beginning of each run.

Carriage velocity was also measured continuously by a DC tachometer driven from a rubber-tired wheel running on the track rails. A more precise measure of velocity was obtained by six photocell-actuated electronic timing clocks, which measured the carriage velocity over 25-foot consecutive intervals along the track. Measurements were consistent and repeatable within ± 1/2 of 1 percent at all velocities tested.

TEST CONDITIONS

The flight conditions tested were selected to simulate STOL takeoff and landing configurations of the full-scale aircraft. All tests were conducted with wing leading edge slats on, flaps extended, tail rotor stopped, and a horizontal stabilizer incidence of 20°. The main propeller blade angle was fixed at a constant value of 12° measured at the 3/4 radius, and model motor power was adjusted to maintain propeller speed of 4000 rpm at all test conditions. The variables in the test program were wing incidence, flap deflection, horizontal velocity, and altitude. Constant-altitude runs were made at nominal altitudes of 4, 10, and 17 inches ground clearance, and varying-altitude runs were made through the range of 3 to 36 inches ground clearance. Lift, drag, and pitching moment were measured. No direct measurement of propeller thrust was made. The thrust coefficient, $C_{T_{,s}}$, was determined by the method described in Appendix I.

TABLE I. SUMMARY OF TEST CONDITIONS

Wing Incidence i_w°	Flap Deflection δ_f°	Velocity V_o ft/sec	Slipstream Thrust Coefficient $C_{T_{,s}}$
30	30	26.0	0.80
-	60	26.1	-
40	30	14.4	0.94
-	-	20.4	0.88
-	60	20.3	-
60	30	13.2	0.95
-	40	18.6	0.90

DISCUSSION OF RESULTS

GENERAL NATURE OF GROUND EFFECT

The nature of ground effect in the flight regime of present interest is typically different from that generally recognized in more conventional flight conditions. The primary influence of the presence of the ground is usually considered to be the reduction of the absolute magnitude of the induced angle of attack at the wing, thereby reducing the induced drag and increasing the lift of the wing.[3] This effect may be calculated by determining the velocity induced at the wing by an imaginary image horseshoe vortex system which replaces the ground plane and satisfies the boundary condition of no through-flow at this plane. This induced velocity, due to the image, is referred to as an influence velocity. Because of practical limitations on angle of attack and lift coefficient, a conventional wing does not operate in conditions where the effect of the bound vortex image is of importance (since it produces primarily a change in horizontal velocity at the real lifting line). Therefore, only the effect of the trailing image pair is normally considered, and only an angle-of-attack change due to its presence is estimated.

For a lifting surface operating at high angles of incidence and/or free-stream lift coefficient, however, the influence of the bound vortex image becomes of real significance.[4,5] The reasons are simply a matter of geometry and order of magnitude of the horizontal influence velocity. Also, under the stated condition of high lift coefficient, the inclination to the free stream of the trailing vortex system (and its image) can no longer be neglected;[7] and a further reduction in horizontal velocity at the real lifting line must be considered, because of the component of the trailing system vorticity perpendicular to the free-stream velocity.*

The net result of including the contributions from the bound vortex and the wake deflection is an influence velocity vector pointing generally forward and upward at the location of the real lifting line. For a wing-propeller system at high incidence, according to the developments in

*The relative importance of the bound vortex and trailing vortices can be readily seen in Figure 15 (taken from Reference 7), where the bound vortex image is the sole contributor to δu at zero wake inclination angle ($\theta = 0^\circ$). The expression for δu given in Reference 7 reduces at $\theta_n = 0$ to that obtained in Reference 4 for the bound vortex image contribution of an elliptically loaded wing. The bound vortex image makes no contribution to δw.

Appendix II, this vector causes a reduction in wing force (and therefore a reduction in remote wind axis lift and drag) and an increase in thrust (a further drag reduction but a lift increase). Thus, it would be expected that for a propeller-driven tilt-wing aircraft, the presence of the ground would typically cause a drag reduction and the possibility of either a decrease or an increase in lift.

EXPERIMENTAL RESULTS

The experimental data taken during this program are presented in Figures 5 through 7. Lift, drag, and pitching moment coefficients based on slipstream dynamic pressure are shown as a function of height of the bottom of the model fuselage above the ground plane for given settings of wing incidence, flap deflection, propeller blade angle, propeller rpm, and flight velocity. Shown for comparison purposes are the steady-state points, with altitude constant, as well as the data taken by quasi-steady-state tests, in which the altitude was programmed to vary slowly during the course of a run. In general, the data taken during the quasi-steady-state runs agree well with the steady-state points and show the continuous variation of the lift, drag, and pitching moment with height.

The trends described in the previous section of the "Discussion of Results" are generally observable in all the test data presented in Figures 5 through 7. Lift variations in either direction can be seen to occur as the altitude changes; however, the drag force always reduces with decreasing altitude.

It is difficult to generalize the anticipated trends in pitching moment. Typically, even out of ground effect, the total pitching moment acting on an aircraft is a combination of many contributory factors, usually large and opposing. An illustration of the complication is presented in Figure 6a. The model fuselage bottom was removed (leaving an open vented cavity) in an attempt to measure the "suck down" due to the pressure distribution on the bottom of the fuselage. The change in ground proximity effect reflected in the measured forces was negligible; however, the difference in pitching moment change due to ground effect was equivalent to more than a 10-percent MAC forward cg shift. The flow under the fuselage bottom is evidently causing a pressure distribution that has little effect on lift and drag but that is contributing, either directly or indirectly, a nose-up moment equivalent to over 75 percent of the allowable cg range of the aircraft.[6]

The magnitude of ground proximity effects appears to increase with increasing flap deflection and wing incidence. The experimental conditions covered are too limited to identify these trends any more selectively; for further insight into the relative importance of the various parameters, it is necessary to consider theoretical methods supported by additional experimental evidence. The developments of Appendix II, based on Reference 7, represent one analytical approach that, although highly simplified, indicates some promise of success in better understanding and predicting ground effect phenomena in this flight regime.

RESOLUTION OF COMPONENT FORCES

Figures 8 through 10 present the data of Figures 5 through 7 in polar form at the ground heights at which constant-altitude runs were made. Included on the graphs are data from similar models measured in other facilities as indicated. In order to gain some insight into the individual contributions of the wing and propeller forces to the total lift and drag produced by the model, some simplifying assumptions are made. As a result of these assumptions, it is possible to separate the forces and to estimate the change of the propeller force and the wing force with height above the ground. This vector resolution is diagrammed in Figure 12, and the results are presented on the polar plots as propeller and wing force vectors. The propeller thrust is shown acting along an average propeller shaft axis, and the wing force is shown acting at the aerodynamic center of the wing. Pitching moment in terms of percent MAC is also presented, as calculated from these two vectors alone compared with the measured values. Certain assumptions are necessary to determine the component forces as described below.

First, consider propeller thrust. In general, the influence of ground proximity can be represented by changes in angle of attack and dynamic pressure at the model. The angle of attack and dynamic pressure changes are determined by the image method described previously. Figure 11 presents experimental data on the variation of propeller thrust of one propeller, in the presence of the wing, on the configuration of interest, as a function of wing incidence (propeller angle of attack) and forward speed. This figure shows that the propeller thrust on this particular configuration, in the flight conditions of interest, does not depend significantly on either dynamic pressure or angle of attack.* Therefore, it is reasonable to assume that in all the data under consideration, the propeller thrust is constant for a given flight condition and does not vary with height above the ground. Also, if it is assumed that the propeller normal force is proportional to the thrust, then the previous argument for constant thrust justifies the neglecting of propeller normal force changes.

Additionally, it is assumed that changes in fuselage forces are negligible compared to changes in wing forces, and then it follows that all of the

*The developments of Appendix I give some insight into the reasons for the insensitivity of thrust to velocity and angle of attack by consideration of wing interference effects.

ground proximity effects are reflected in changes in the wing forces. Partial justification for the neglect of fuselage forces is shown by Figure 6a, where removal of the lower half of the fuselage produced little change in the total forces. It would be expected that in the test conditions of interest, where the free-stream dynamic pressure is small, the fuselage forces are small.

As a result of the above assumptions, the data of Figures 8 through 10 can be resolved into two forces, propeller thrust acting along the propeller shaft and wing force acting at the 25-percent MAC. The propeller thrust is determined from Figure 11 for all heights above the ground and is subtracted from the measured resultant force C_{F_S}, to determine the wing force C_{W_S}.

The resolved polar plots indicate a large percentage change in wing force magnitude and direction produced by ground effects in some of the cases tested. Particularly in the high C_{T_S} conditions, near trim (i.e., $C_{D_S} \cong 0$), the wing force changes as much as 50 percent in magnitude and rotates more than 30° (Figure 10a).

In addition, the variations in pitching moment due to ground effect, as determined by the resolved propeller and wing forces, generally agree in sign and magnitude with the measured increments. As Figure 6a indicates, however, the flow along the fuselage bottom has a profound effect on the moment change due to ground effect. The indication is that the pitching moment, typically a balance of several rather large effects, cannot be allocated to one principal source, as can the force effects.

COMPARISON OF DATA SOURCES

The data from some of the references[9,10] are as yet unpublished and should be considered as preliminary. Where possible, published data (typically out of ground effect) from the same source have been presented as a reference. With the exception of data from Reference 8 (presented in Figure 6b), it is difficult to make further comparisons of pitching moment data either because of differences in thrust line location (as in the model of Reference 9) or because the tests were conducted in the tail-off configuration (Reference 10). The data source comparison will therefore be confined to consideration of force changes due to ground effect.

When making a comparison of the influence of ground proximity in different types of test facilities, it is important to note that a significant difference in testing technique is present. In the case of the Dynamic Model Track tests, forces and moment were measured at various altitudes while propeller blade angle and advance ratio were held constant (in fact, both model rpm and forward velocity were held constant). In the wind tunnel tests, either rpm or tunnel speed was adjusted to maintain a constant ratio of propeller disc loading to free-stream dynamic pressure (i.e., constant C_{T_S}) at the various altitudes.

In the former case, any influence of ground proximity on the propeller thrust is included in the measured forces and moment. In the latter (specifically when thrust is held constant at constant tunnel speed), the effect of this influence is eliminated. The fact that the former technique is more representative of the actual aircraft in flight need not be emphasized in the present discussion, but it should be considered in applying the data to flight conditions.*

Due to the light construction necessary for dynamic models, it was not possible to provide direct, accurate measurement of propeller thrust in the experiments performed in the Dynamic Model Track. In order to calculate thrust coefficient based on slipstream dynamic pressure and to compare the results presented here with those from other facilities, it was necessary to estimate the propeller thrust. The analytical method by which the propeller thrust was determined is described in Appendix I.

The following comments are based on comparison of the data at the same values of thrust coefficient (based on slipstream dynamic pressure) where, for the data presented here, the thrust was determined by a combination of analytical techniques and experimental data as described in Appendix I.

In both wind tunnel and Dynamic Model Track facilities, the trend of the force change due to ground effect in this flight regime may be thought of as a forward rotation (reducing drag) and a decrease in magnitude of the resultant aerodynamic force vector. The major difference observed in the data from the two types of facilities appears to be not in the nature of the ground effect, but rather in its magnitude. The wind tunnel tests typically exhibit a greater force change due to ground effect than do the Dynamic Model Track tests. The difference appears as a combination of greater rotation and more magnitude reduction of the resultant aerodynamic force vector.

In Figures 8b, 9c, and 10b can be seen the effect on the force data due to the operation of a moving belt ground plane on the wind tunnel floor. These data, taken from Reference 10, indicate that, although use of the moving belt brings the in-ground-effect data into closer agreement between the two facilities, a noticeable discrepancy still exists.

*Even though the experimental data of Figure 11 show a reduced sensitivity of thrust to velocity and angle of attack, significant thrust changes in ground effect may occur according to the developments of Appendix I. The nature of the propeller thrust variation in ground effect will depend upon the test conditions.

The comparison is most easily discussed in terms of the resolved wing force defined previously. For example, consider Figure 10b, where the out-of-ground-effect data from three different facilities and models are in substantial agreement. Three effects are apparent:

1. The Dynamic Model Track wing force data show a greater rotation due to ground effect than do the wind tunnel data.
2. The wind tunnel data taken without a moving belt show a greater wing force reduction than do the Dynamic Model Track data.
3. The wind tunnel data taken with a moving belt indicate a wing force in ground effect that is approximately the average of the Dynamic Model Track data and the wind tunnel data taken without a moving belt.

A possible explanation for the first of these observations is that, although the propeller thrust was assumed to be constant with altitude, as the altitude decreases, the thrust, in fact, increases in the Dynamic Model Track tests (as discussed in Appendix II). This will result in an apparent wing force rotation in the Dynamic Model Track tests, whereas in the wind tunnel tests the thrust is actually held constant and this apparent rotation is not present. The remaining two effects are less easily explained, but they might be due to the presence of a boundary layer on the wind tunnel ground plane producing an average velocity at the model less than that calculated from the test section instrumentation. Thus, the tests in ground effect are actually being performed at a higher $C_{T,_S}$ (lower velocity) than indicated, and the force coefficients appear correspondingly smaller (the effect of $C_{T,_S}$ on the wing force coefficient is presented in Figures 9a and 9b, where it can be seen that increasing $C_{T,_S}$ reduces $C_{W,_S}$). Operation of the moving belt ground plane apparently reduces the magnitude of this effect but does not completely eliminate it. In Figures 8b and 9c, the difference between the Dynamic Model Track test data and the wind tunnel with moving belt test data is more pronounced; however, the out-of-ground-effect data are not in as good agreement as in Figure 10b, and the comparison is therefore more difficult. In these cases, the wing force change due to ground effect in the moving belt tests is almost twice the change observed in the moving-model tests.

It has been observed from photographs of tufts on the floors of the two types of facilities (conventional wind tunnel and Dynamic Model Track) that the downwash disturbance produced by the model propagates considerably farther upstream in a wind tunnel than in a moving-model facility under supposedly identical test conditions. The relationship between test conditions, type of facility, and upstream position of this disturbance front has not been determined. If it is assumed that the disturbance front is a line where the local slipstream dynamic pressure equals the local free-stream dynamic pressure, then at constant propeller thrust, the front position is a measure of the local free-stream dynamic pressure (assuming a diffusing slipstream emanating from the model). Thus, the

more forward position of the disturbance front in the wind tunnel tests would indicate a lower free-stream dynamic pressure. The position of the disturbance front at other than floor level has not been established; thus, a quantitative determination cannot be made as to how much the boundary layer influences the average test section velocity at the model and consequently how the experiment is influenced by the moving belt operation.

CONCLUSIONS

1. The experimental data presented indicate that ground effects on longitudinal forces and pitching moment can be pronounced in STOL flight conditions. The trend of test data is toward net reduction of both lift and drag with decreasing altitude, with lift showing local increases and drag exhibiting a constant trend of decreasing with altitude. Pitching moment data typically indicate a net nose-down moment change. The analysis indicates that the moment change is partly due to wing and propeller force variations. Other, more complicated effects such as flow under the fuselage bottom and change in the downwash at the tail were not calculated, but they are also contributing factors.

2. Comparison of data from wind tunnel tests with data from moving-model tests, as reported herein, indicates that the latter, more accurate simulation technique shows less force change due to ground effect. In identical test conditions, where ground proximity effects are severe, lift reduction in moving-model tests is as little as one-third the lift reduction shown by wind tunnel tests, and drag change in moving-model tests is approximately one-half the change shown in wind tunnel tests. The one pitching moment comparison possible indicated a moving-model test change of about one-half the wind tunnel test change. Wind tunnel tests with a moving belt on the ground plane show closer agreement with the moving-model tests; however, some test cases indicate a force change due to ground effect in the moving belt tests that is about twice the change observed in moving-model tests.

3. A distinct difference was observed in the distance upstream that the flow disturbances caused by the model propagate as indicated by the behavior of tufts on the floor of a wind tunnel and the Dynamic Model Track. Typically, the position of the disturbance area was much farther upstream in the wind tunnel tests than in the moving-model tests, indicating a velocity defect due to tunnel boundary layer that could influence the data.

RECOMMENDATIONS

The problems of defining an adequate wake model and predicting the aerodynamic forces acting on a wing immersed in the slipstream should be investigated further.

To pursue the aim of formulating design prediction techniques, it is necessary that comprehensive experimental studies be made using a model with separable propeller and wing force and moment instrumentation, both in and out of ground effect. Particularly in ground effect, it is mandatory that precise simulation of actual flight conditions be maintained; otherwise, additional prediction problems arise which are associated with tunnel boundary layer effects. Suitable flow visualization techniques should be employed to observe the wake position and character as functions of the test variables. In conjunction with the experimental effort, analytical studies should be pursued to refine the theoretical approach and to accommodate the more extensive experimental observations.

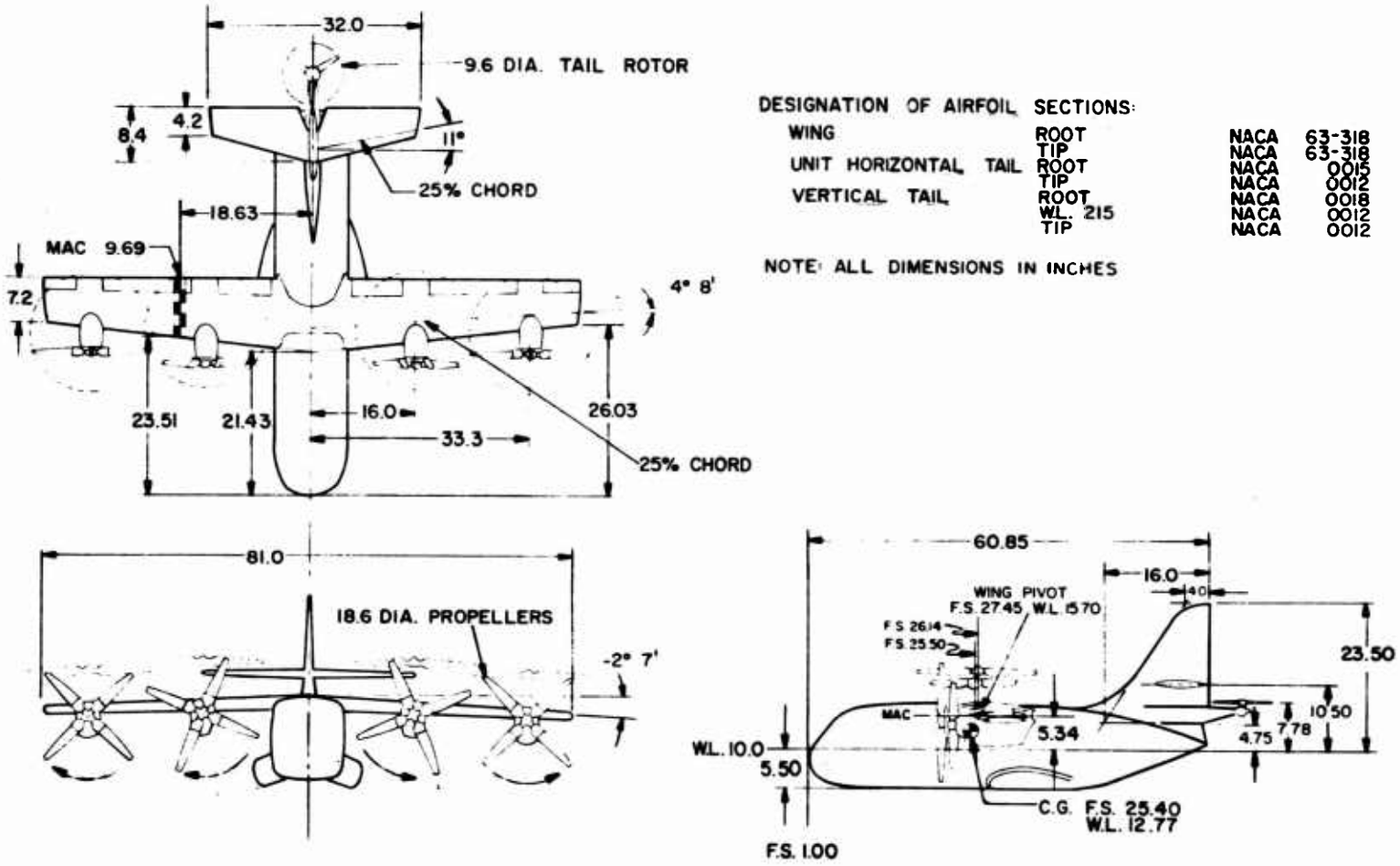

Figure 3. General Arrangement, One-Tenth Scale XC-142 Model.

Note: Wing Airfoil Section NACA 63-318
Angular Travel of Vane = 1.075 x Angular Travel at Flap
All Dimensions Given in Percent Chord at Any Wing Station

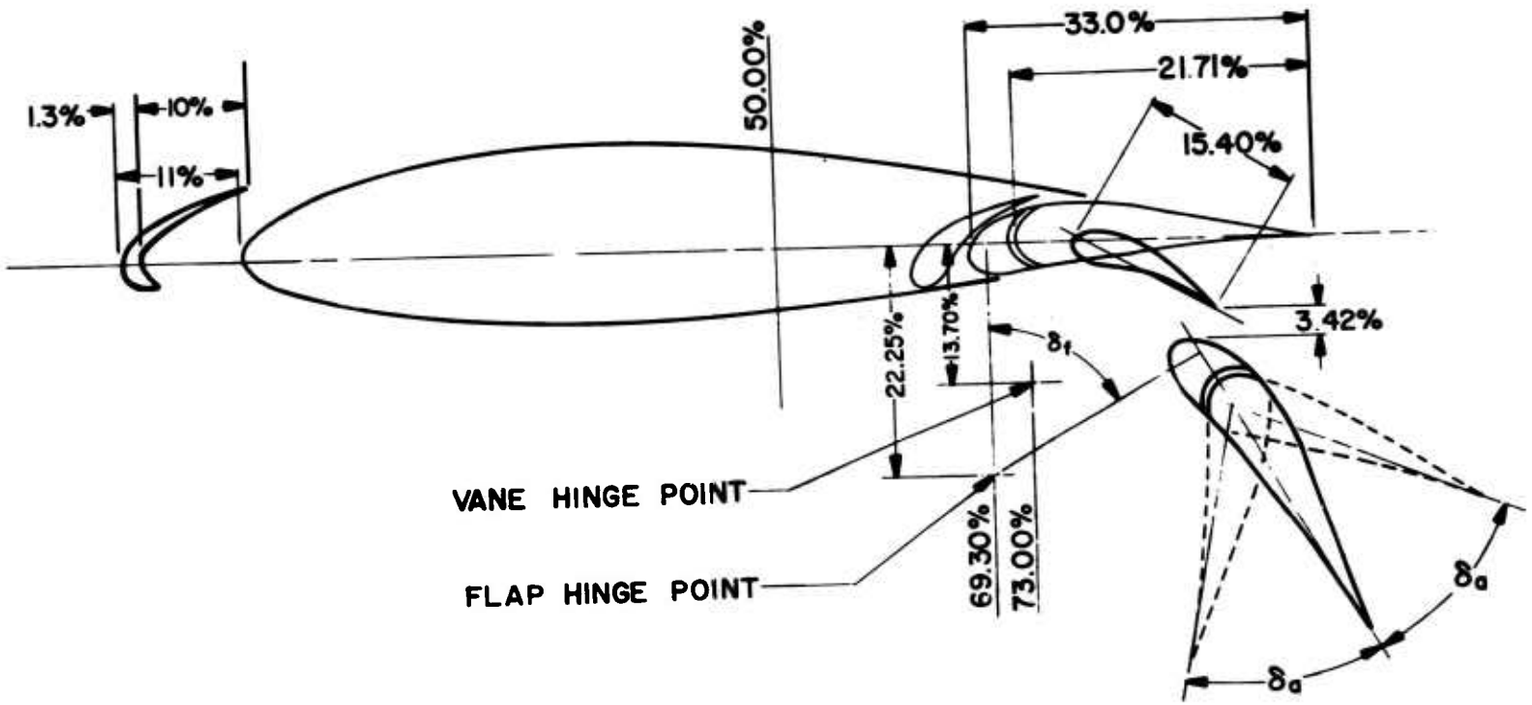

Figure 4a. Flap and Slat Arrangement.

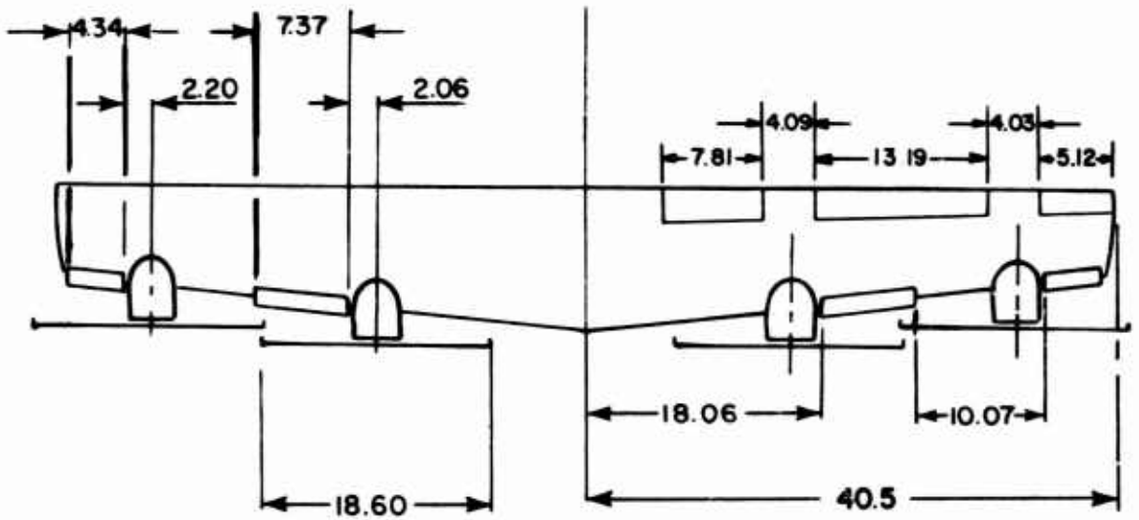

Note: All Dimensions are in inches

Figure 4b. Spanwise Location of Flaps and Slats.

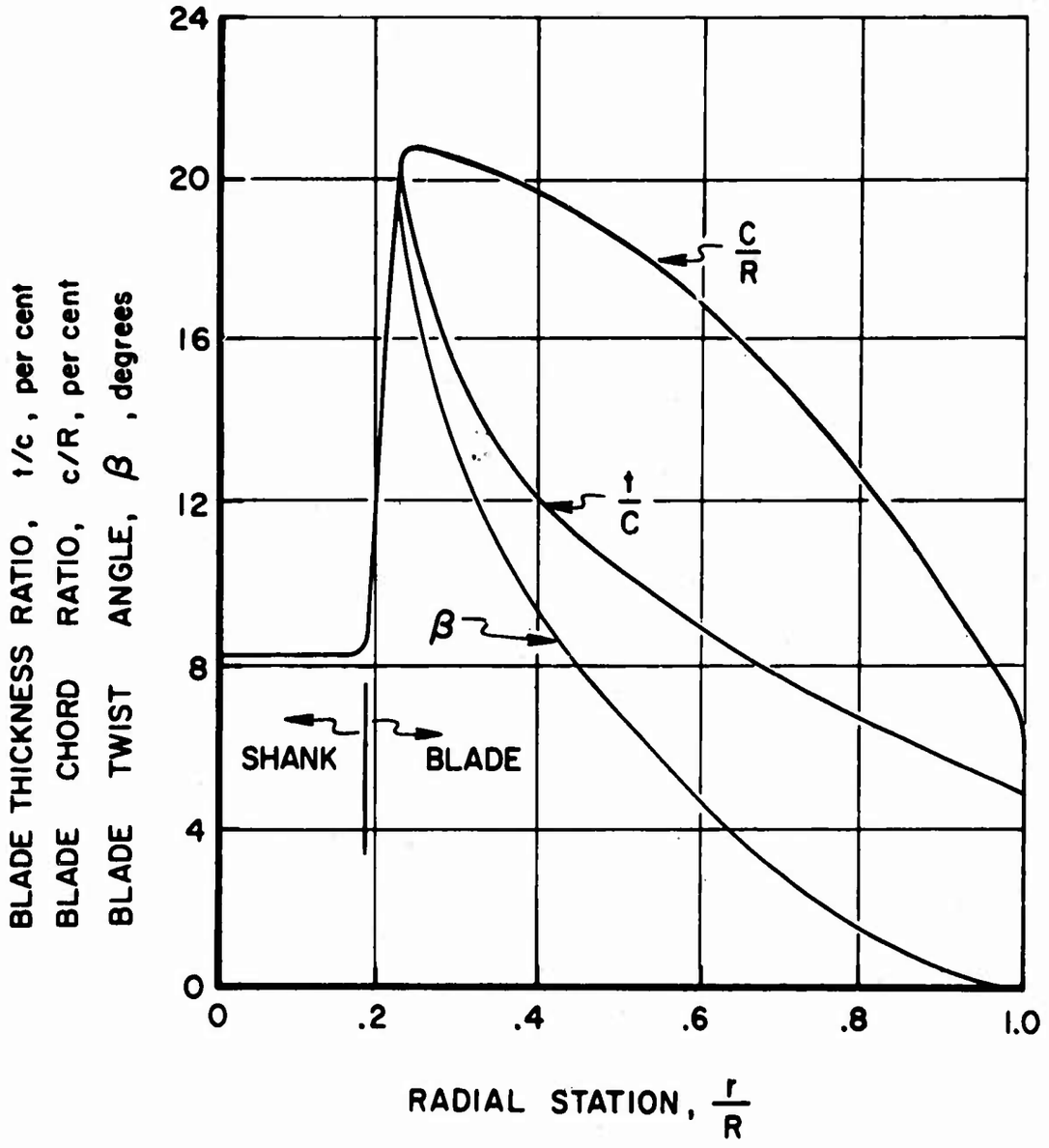

Figure 4c. Propeller Blade Characteristics, Four Blades.

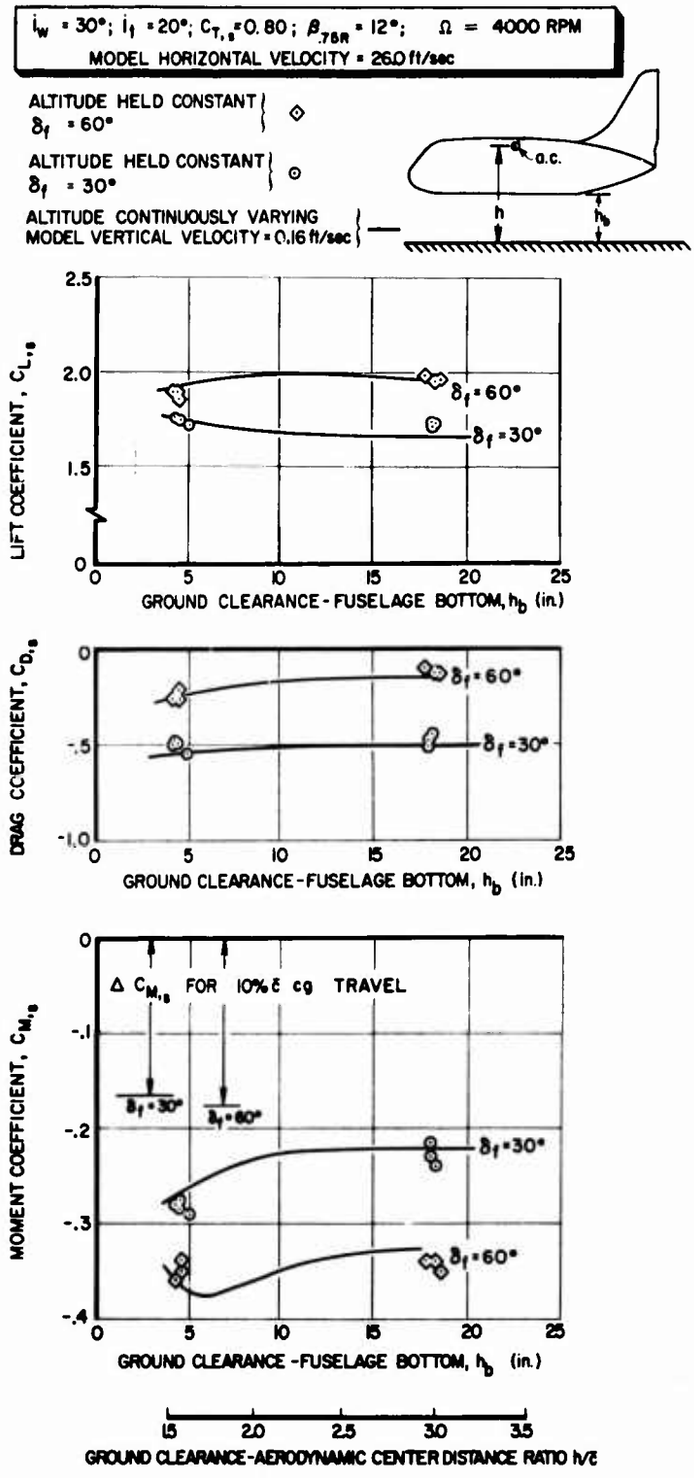

Figure 5. Experimental Data; Effect of Ground Proximity on Model Forces and Pitching Moment, $i_w = 30°$.

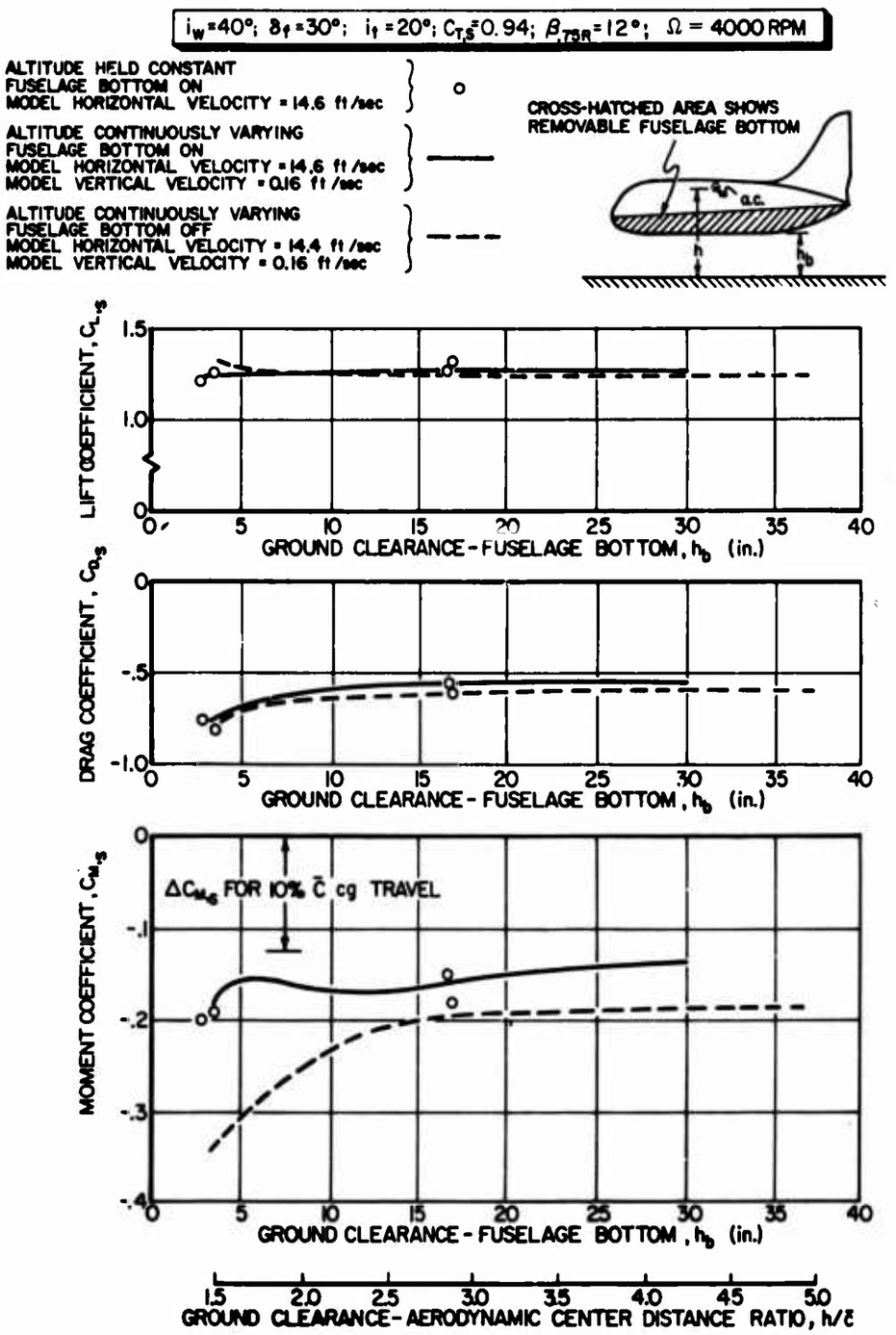

Figure 6a. Experimental Data; Effect of Ground Proximity on Model Forces and Pitching Moment, Including Effect of Removing Fuselage Bottom, $i_w = 40°$.

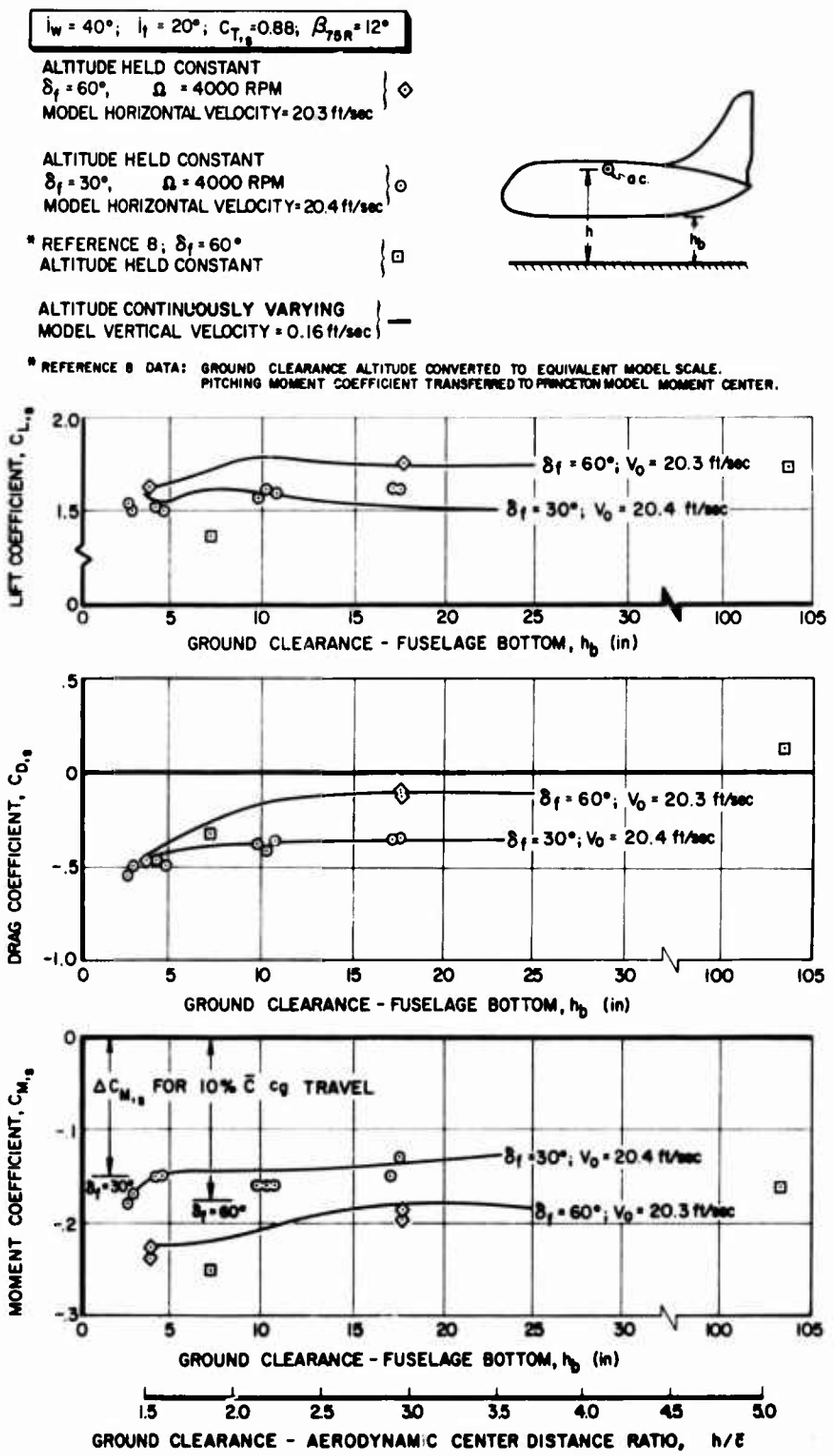

Figure 6b. Experimental Data; Effect of Ground Proximity on Model Forces and Pitching Moment, $i_w = 40°$.

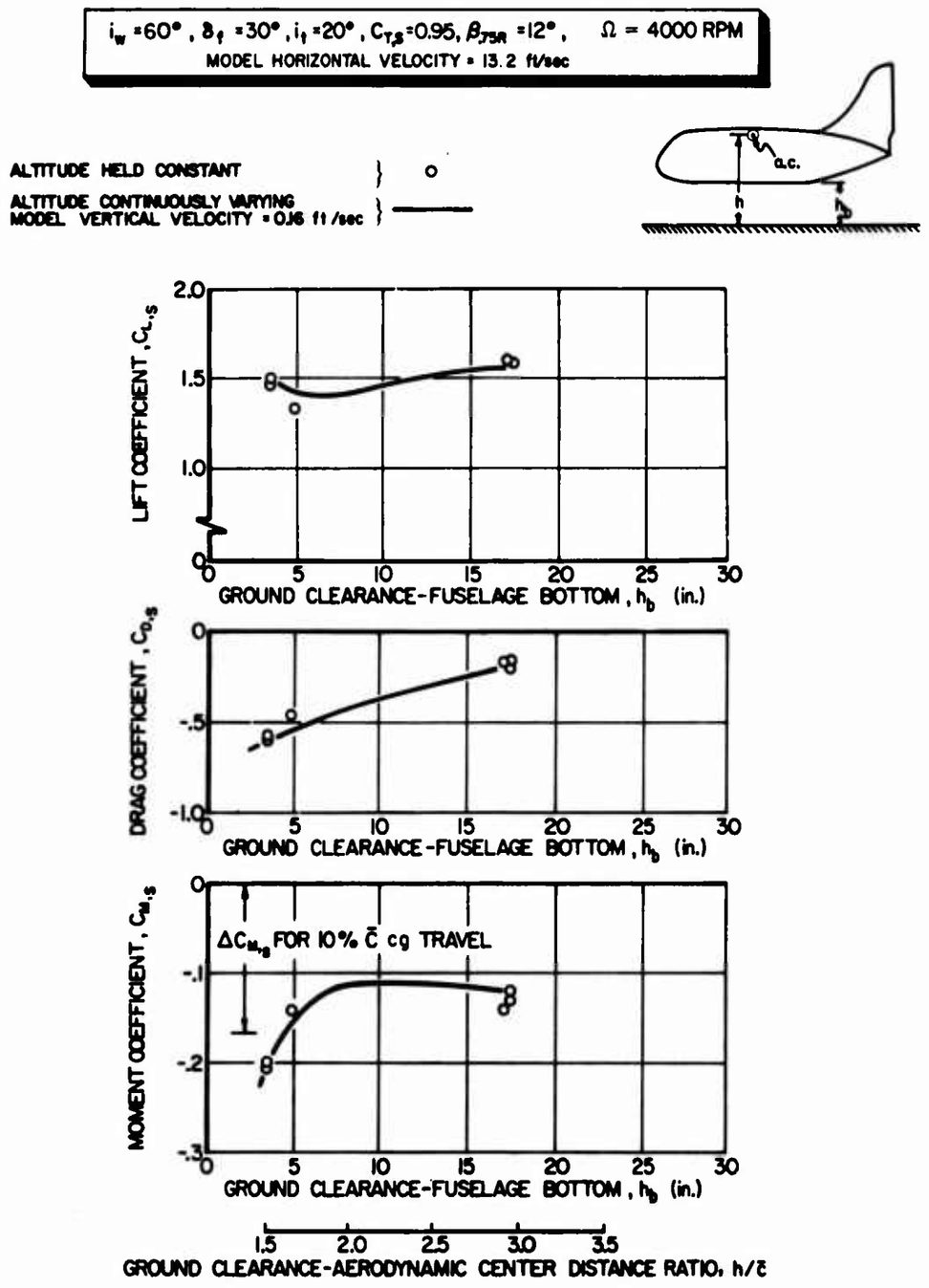

Figure 7. Experimental Data; Effect of Ground Proximity on Model Forces and Pitching Moment, $i_w = 60°$.

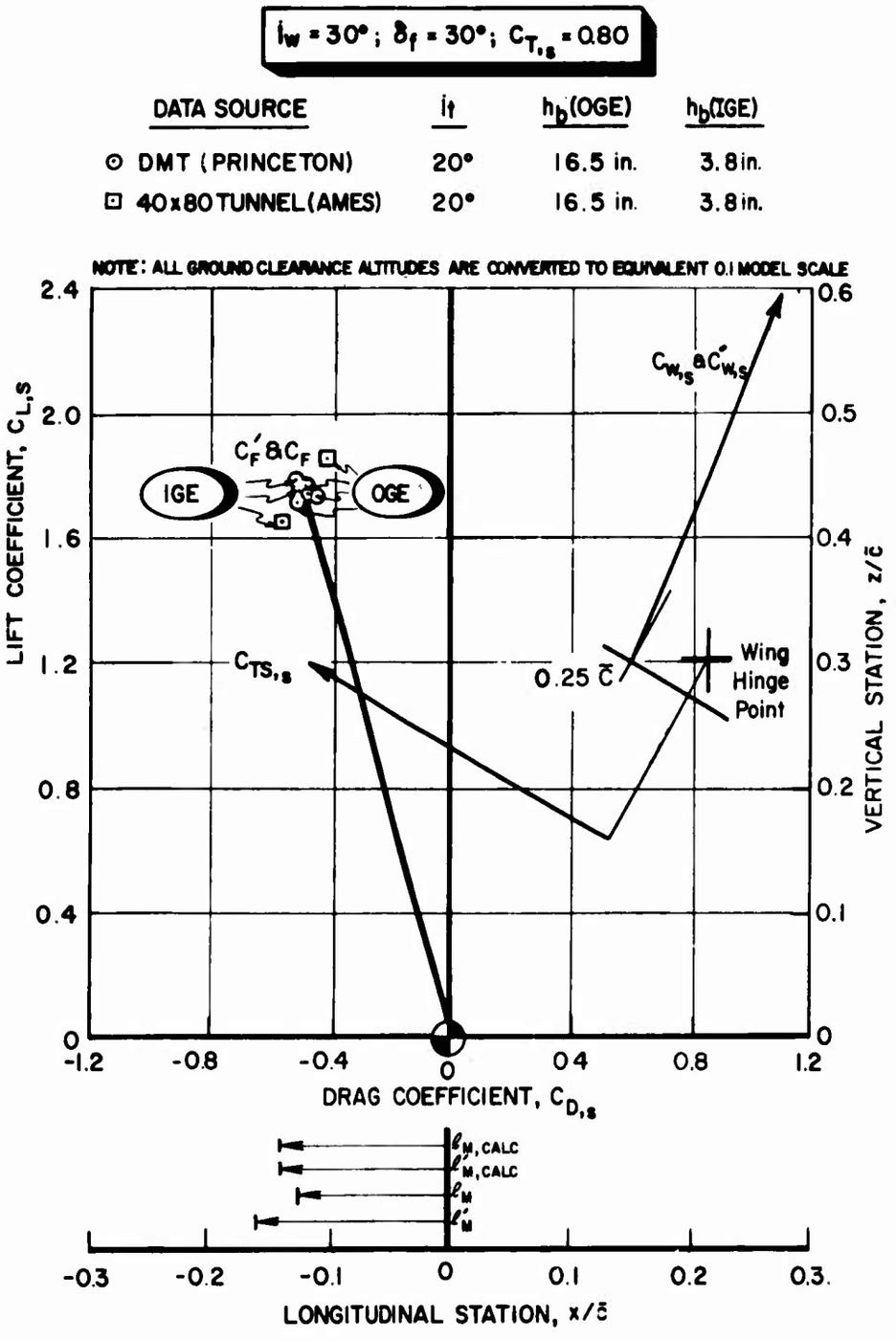

Figure 8a. Ground Effect; Component Contributions and Comparison With Wind Tunnel Values, $i_w = 30°$.

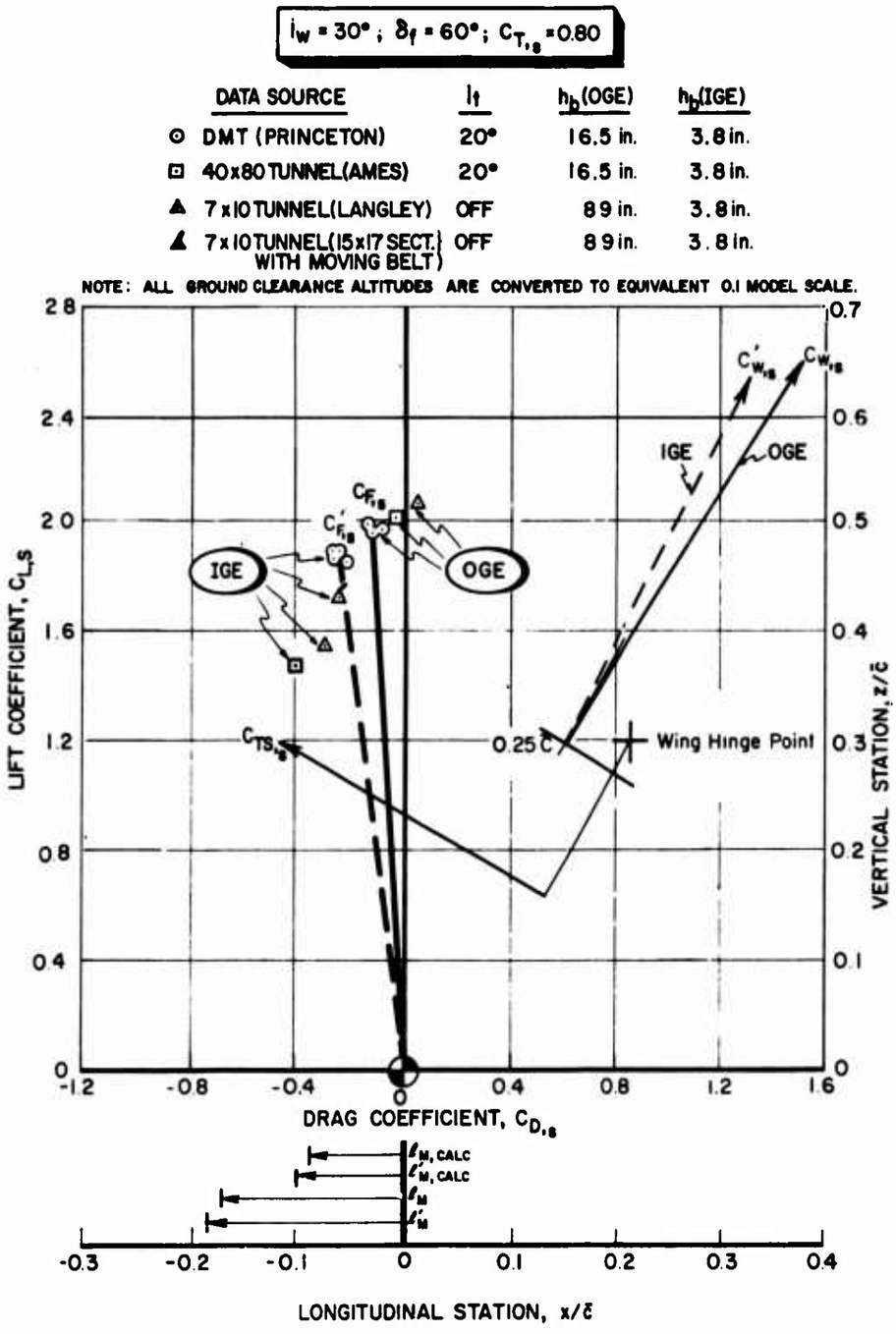

Figure 8b. Ground Effect; Component Contributions and Comparison With Wind Tunnel Values, $i_w = 30°$.

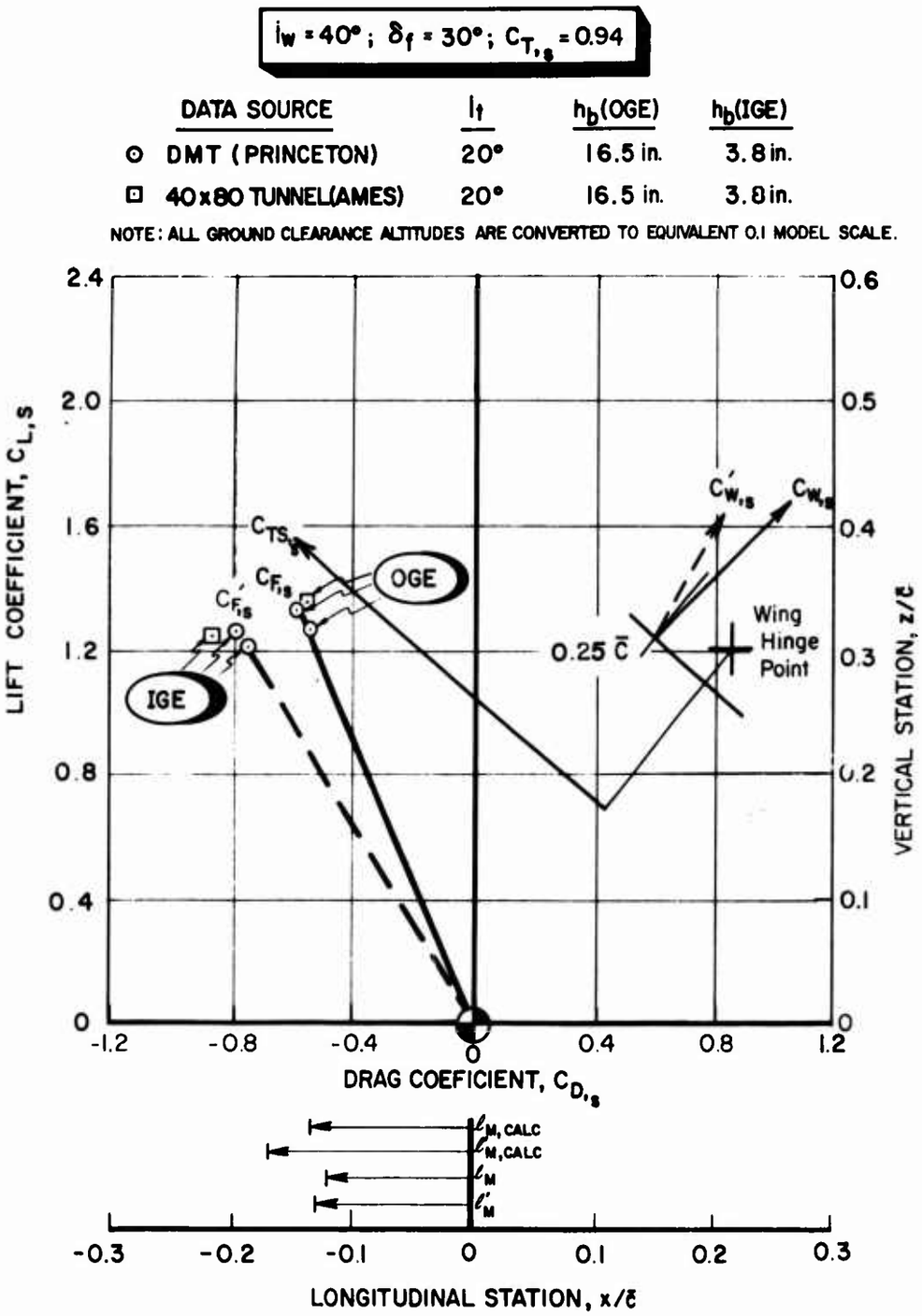

Figure 9a. Ground Effect; Component Contributions and Comparison With Wind Tunnel Values, $i_w = 40°$.

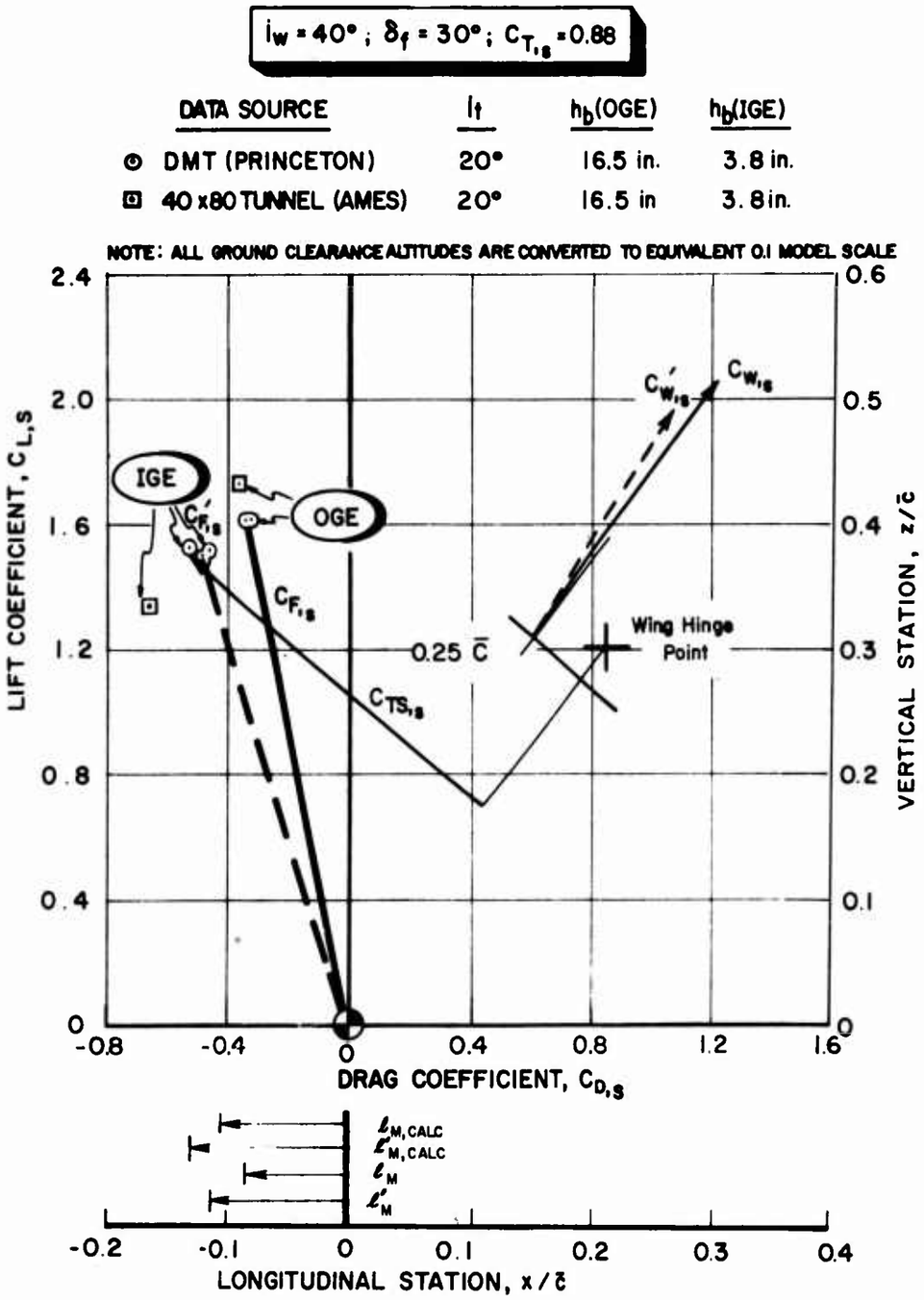

Figure 9b. Ground Effect; Component Contributions and Comparison With Wind Tunnel Values, $i_w = 40°$.

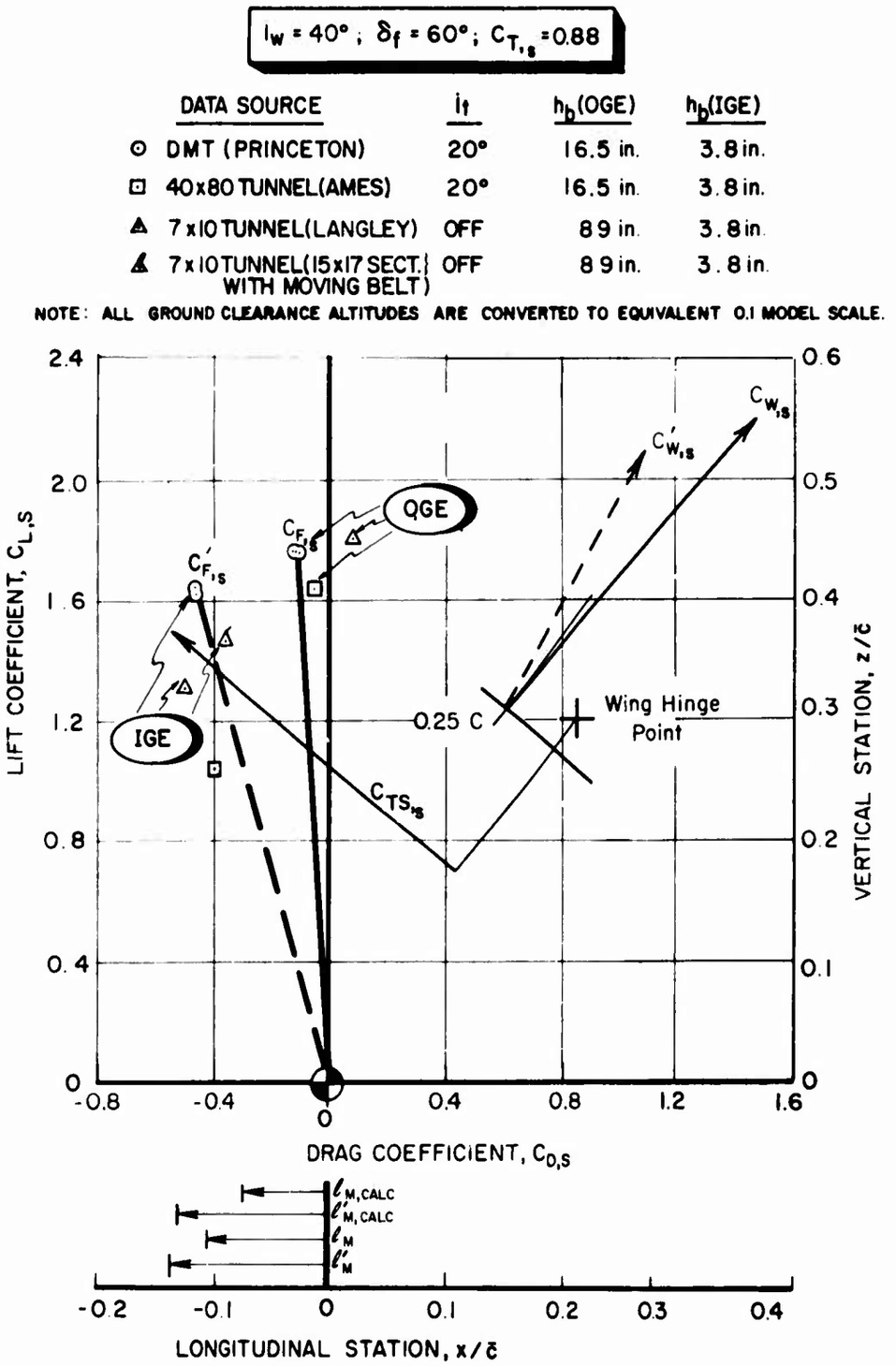

Figure 9c. Ground Effect; Component Contributions and Comparison With Wind Tunnel Values, $i_w = 40°$.

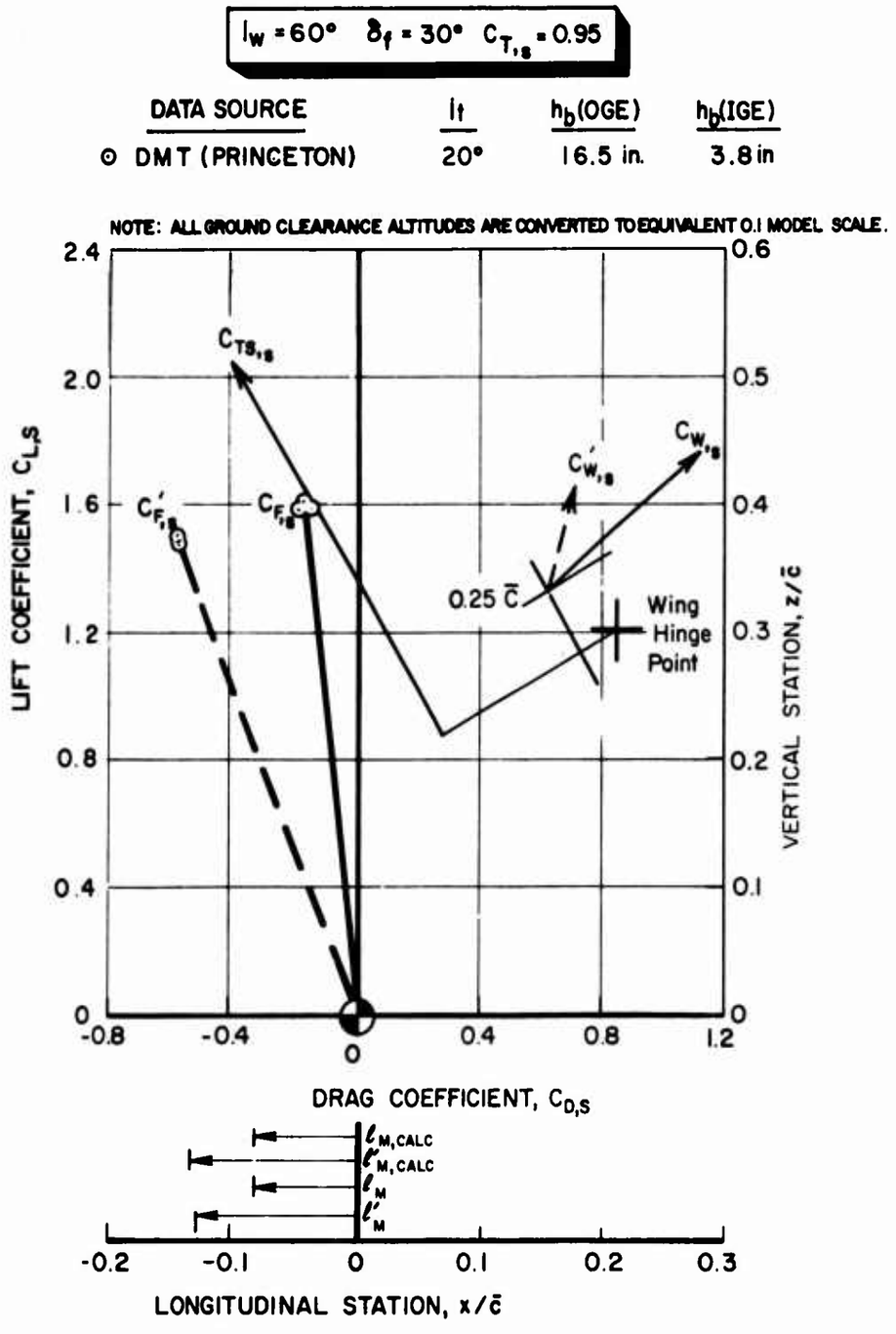

Figure 10a. Ground Effect; Component Contributions and Comparison With Wind Tunnel Values, $i_w = 60°$.

$i_w = 60°$; $\delta_f = 40°$; $C_{T,s} = 0.90$

DATA SOURCE	i_t	h_b(OGE)	h_b(IGE)
⊙ DMT (PRINCETON)	20°	16.5 in.	3.8 in.
⊡ 40x80 TUNNEL(AMES)	20°	16.5 in.	3.8 in.
△ 7x10 TUNNEL(LANGLEY)	OFF	89 in.	3.8 in.
◭ 7x10 TUNNEL(15x17 SECT. WITH MOVING BELT)	OFF	89 in.	3.8 in.

NOTE ALL GROUND CLEARANCE ALTITUDES ARE CONVERTED TO EQUIVALENT 0.1 MODEL SCALE.

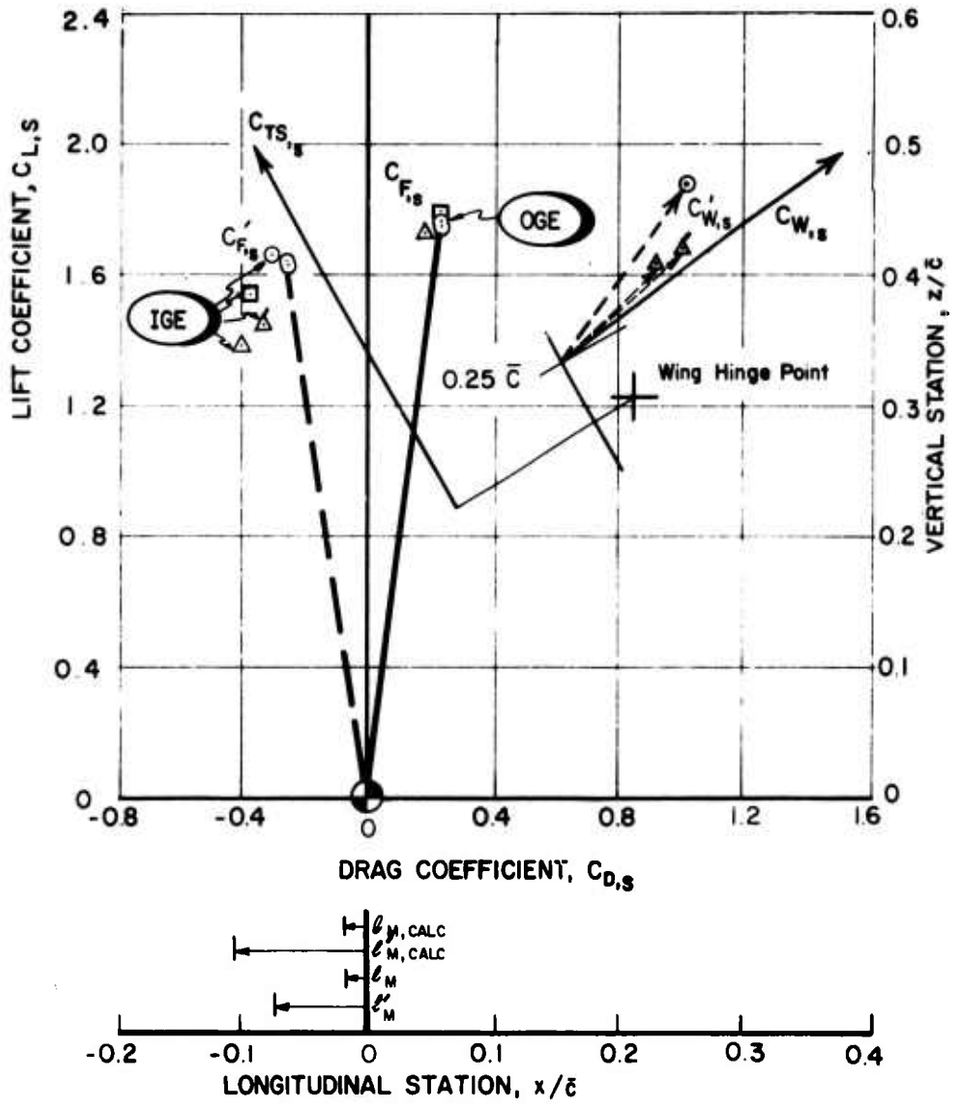

Figure 10b. Ground Effect; Component Contributions and Comparison With Wind Tunnel Values, $i_w = 60°$.

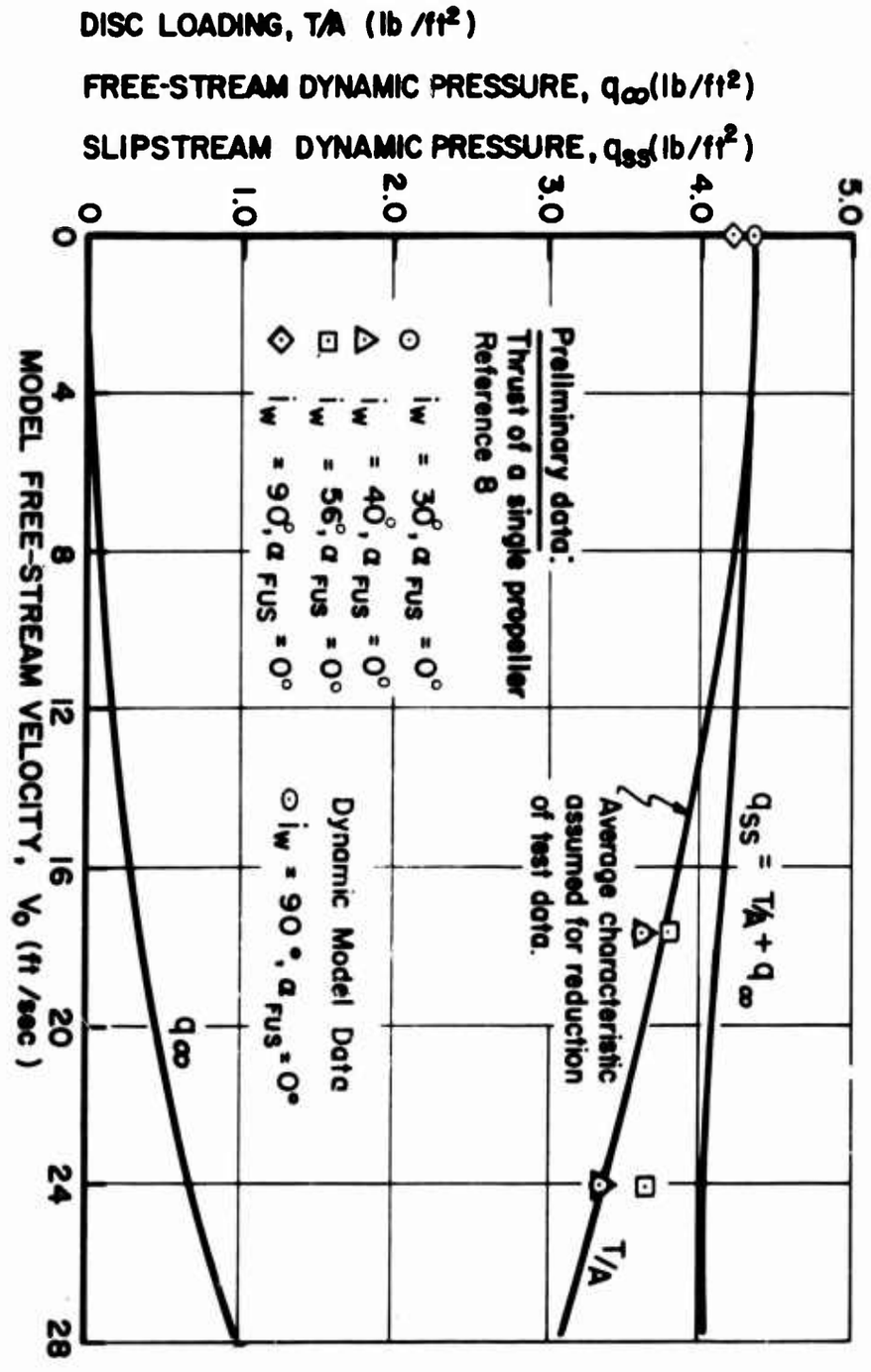

Figure 11. Experimental Thrust Characteristics of One Propeller of Reference 8 Model. Converted to One-Tenth Scale. (Used for Reduction of all Dynamic Model Track Data)

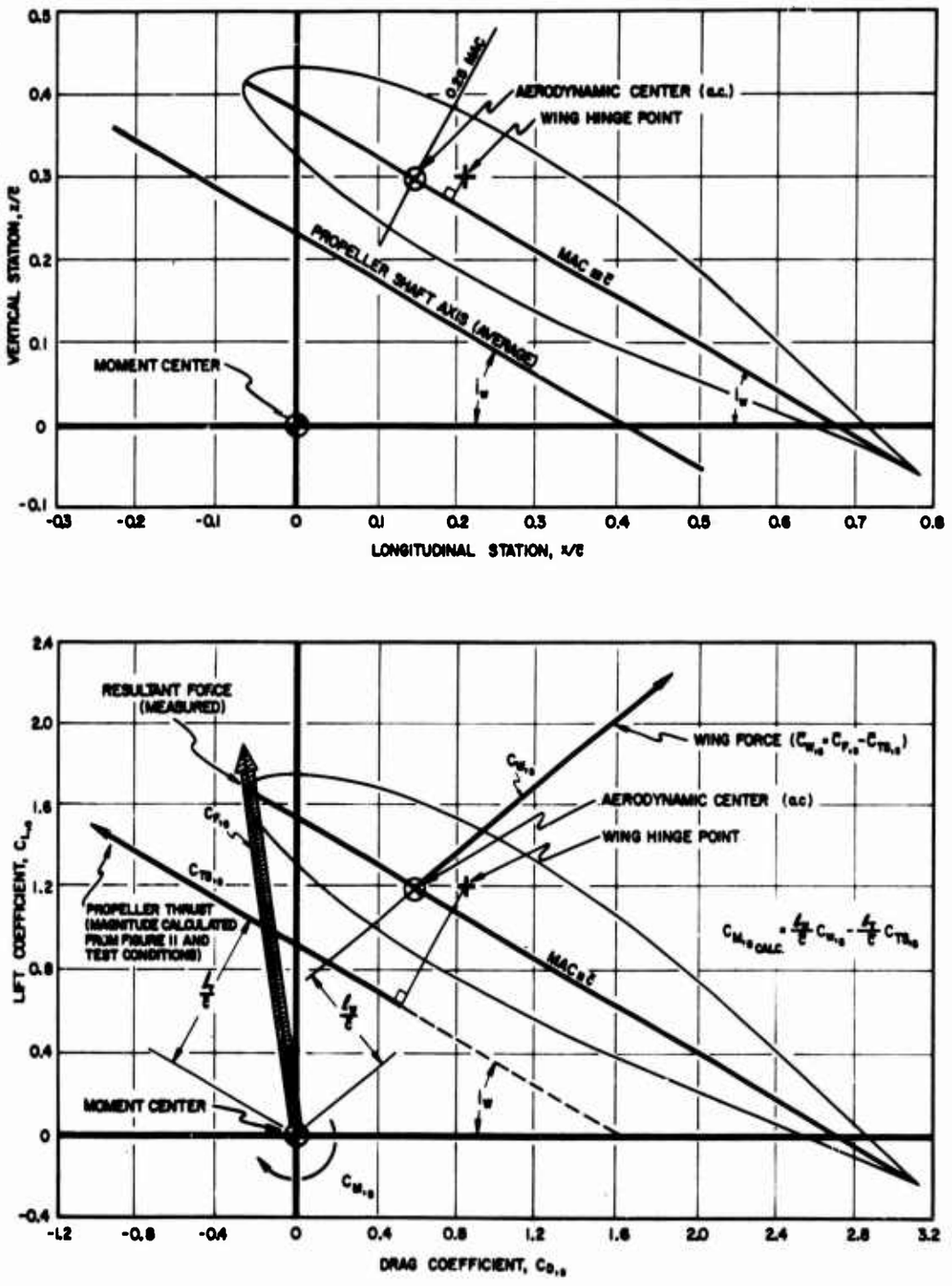

Figure 12. Diagram of Component Force Resolution.

REFERENCES

1. Curtiss, H. C., Jr., Putman, W. F., and Lebacqz, J. V., AN EXPERIMENTAL INVESTIGATION OF THE LONGITUDINAL DYNAMIC STABILITY CHARACTERISTICS OF A FOUR-PROPELLER TILT-WING VTOL MODEL, Princeton University; USAAVLABS Technical Report 66-80, U. S. Army Aviation Materiel Laboratories, Fort Eustis, Virginia, September 1967, AD 663848.

2. Curtiss, H. C., Jr., Putman, W. F., and Traybar, J. J., GENERAL DESCRIPTION OF THE PRINCETON DYNAMIC MODEL TRACK, Princeton University; USAAVLABS Technical Report 66-73, U. S. Army Aviation Materiel Laboratories, Fort Eustis, Virginia, November 1966, AD 645883.

3. Glauert, H., AEROFOIL AND AIRSCREW THEORY, Cambridge University Press, 1926.

4. Bairstow, Leonard, APPLIED AERODYNAMICS, Second Edition, New York, Longmans, Green and Co., 1939, pp. 410-416.

5. Westwater, F. L., THE ROLLING UP OF THE SURFACE OF DISCONTINUITY BEHIND AN AEROFOIL OF FINITE SPAN, Technical Report of the Aeronautical Research Committee 1935-36, Vol. 1, 1937, pp. 116-131.

6. Shields, M. E., ESTIMATED FLYING QUALITIES XC 142A V/STOL ASSAULT Transport, LTV Vought Aeronautics Division; Report No. 2-53310/4R939, LTV Aerospace Corporation, Dallas, Texas, May 1964, p. 22.

7. Heyson, Harry H., LINEARIZED THEORY OF WIND-TUNNEL JET-BOUNDARY CORRECTIONS AND GROUND EFFECT FOR VTOL-STOL AIRCRAFT, Langley Research Center; NASA Technical Report R-124, National Aeronautics and Space Administration, Washington, D. C., 1962.

8. Goodson, Kenneth W., LONGITUDINAL AERODYNAMIC CHARACTERISTICS OF A FLAPPED TILT-WING FOUR-PROPELLER V/STOL TRANSPORT MODEL, Langley Research Center; NASA Technical Note D-3217, National Aeronautics and Space Administration, Washington, D. C., February 1966.

9. PRELIMINARY TEST RESULTS FROM NASA AMES RESEARCH CENTER 40' x 80' WIND TUNNEL, Test No. 178, Moffett Field, California, Unpublished.

10. PRELIMINARY WIND TUNNEL TEST RESULTS FROM NASA LANGLEY RESEARCH CENTER MOVING BELT FACILITY, Test No. 118, Langley Field, Virginia, Unpublished.

11. Prandtl, L., and Tietjen, O. G., FUNDAMENTALS OF HYDRO- AND AEROMECHANICS, New York, McGraw-Hill Book Company, Inc., 1934.

12. Spreiter, John R., and Sacks, Alvin H., THE ROLLING UP OF THE TRAILING VORTEX SHEET AND ITS EFFECT ON THE DOWNWASH BEHIND WINGS, Journal of the Aeronautical Sciences, Vol. 18, No. 1, January 1951, pp. 21-32.

13. Putman, W. F., RESULTS OF EXPERIMENTS ON A TILT WING VTOL AIRCRAFT USING THE PRINCETON UNIVERSITY FORWARD FLIGHT FACILITY, Princeton University; Report No. 542, Princeton, New Jersey, May 1961.

14. Gessow, Alfred, and Myers, Garry C., Jr., AERODYNAMICS OF THE HELICOPTER, Third Printing, New York, Frederick Ungar Publishing Co., May 1967.

APPENDIX I
DETERMINATION OF MODEL PROPELLER THRUST

In order to analyze the data obtained in this research and to present them in a form that is comparable to data from other sources, it was necessary to estimate the propeller thrust developed by the model propellers in these experiments at various test conditions. Because of weight limitations on the dynamic model used, it was not possible to instrument the model for propeller thrust measurements. This estimate was made by scaling propeller thrust from preliminary data taken on one propeller of the model of Reference 10 to the proper size for the model used in the Dynamic Model Track tests.

It was assumed that the thrust coefficient solidity ratio, $\frac{C_T}{\sigma}$, of both the propellers used in the Dynamic Model Track tests and in the tests of Reference 10 was the same function of advance ratio, μ, propeller angle of attack, α_p, and effective blade angle at 3/4 radius, β_e. The effective blade angle was defined as the value of the blade angle that satisfies the combined momentum-blade element theory equation in the static case.[14]

$$\beta_e \equiv \frac{6C_T}{a\sigma} + \frac{3}{2}\sqrt{\frac{C_T}{2}} \qquad (1)$$

The thrust coefficient was calculated from experimental measurements of static thrust. This procedure should approximately take into account the differences in induced velocity variation across the disc of the propeller due to differences in blade twist and planform as well as differences in angle of zero lift of the propeller blades. Then, the thrust produced by the Dynamic Model Track model propellers was determined by knowledge of the test conditions, the effective blade angle determined by equation (1) for each of the propellers, and the experimentally measured C_T of the Reference 10 propeller.

The results of this procedure are presented in Figure 13 as plots of propeller disc loading, T/A, as functions of velocity and wing incidence (at $\alpha_{FUS} = 0$). The dimensions correspond to those for the one-tenth scale Dynamic Model Track model. Also included on this plot are points representing the average disc loading of all four propellers of the identical model used in Reference 10, but measured during the test program reported in Reference 8. The difference between the thrust of a single propeller and the average values is due to a spanwise variation of the measured individual propeller thrust encountered during the tests of Reference 8.

An interesting aspect of the data presented in Figure 11 is the relative insensitivity of propeller thrust to changes in velocity and angle of attack. For comparison purposes, the same data are presented in Figure 13 and compared to a theoretical estimate of the disc loading based on the equation[14]

$$\frac{T}{A} = \frac{\rho a \sigma (\Omega R)^2}{2} \left(\frac{\beta_e}{3} + \frac{\lambda}{.2} \right) \tag{2}$$

In an attempt to explain the rather large difference between the observed and theoretical values of thrust and the dependence of thrust on velocity and angle of attack, consideration was given to the influence of the presence of the wing behind the propellers. This was approached by representing the wing as a "horseshoe" vortex system and computing the velocity induced at the propeller due to this vortex system. Based on the theoretical variation of propeller thrust with velocity and angle of attack, the thrust was corrected for the wing flow field; the corrected points are indicated in Figure 13. Although the corrected theory does not completely account for the experimental observations, it does indicate the proper trend of decreased thrust sensitivity to velocity and angle of attack. The approximation that the wing is represented by a bound vortex line may be overly simplified since the propeller is considerably less than a chord length away from the wing.

The application of the correction is best explained by the vector diagrams of Figure 14. The circulation of the horseshoe vortex system, Γ, is assumed to be constant for simplicity and is determined by the Kutta-Joukowsky lift theorem[11] as

$$\Gamma = \frac{L_W}{\rho V_{R_o} b} \tag{3}$$

As shown in Figure 14, V_{R_o} is the vector sum of the free-stream velocity, V_o; the fully developed propeller induced velocity, $2v_o$; and the wing trailing vortex induced velocity, Δw_{TV}. The wing lift, L_W, is determined by assuming that the aircraft is trimmed (net drag equals zero) and that the wing lift acts perpendicular to the wing chord. Thus,

$$L_W = \frac{T}{\tan i_w} \tag{4}$$

and the experimental value of T is used to find both L_W and V_{R_o}. Figure 14 shows the graphical technique used to determine the corrected velocity and angle of attack at the propeller location due to the velocity induced by the vortex system. The induced velocity was found at an

"average" propeller location midway between the two propellers, and the Biot-Savart Law[11] was applied at this location for the bound vortex and semi-infinite trailing vortices of constant circulation Γ. The use of an "average" propeller location is a simplification that neglects the fact that the velocity induced by the wing bound vortex is not a linear function of distance from the vortex line. The accuracy of this simplification and the neglect of the distribution of velocity and angle of attack across the propeller disc are comparable; both assumptions are commensurate in accuracy with assuming that the wing can be represented simply as a single line vortex.

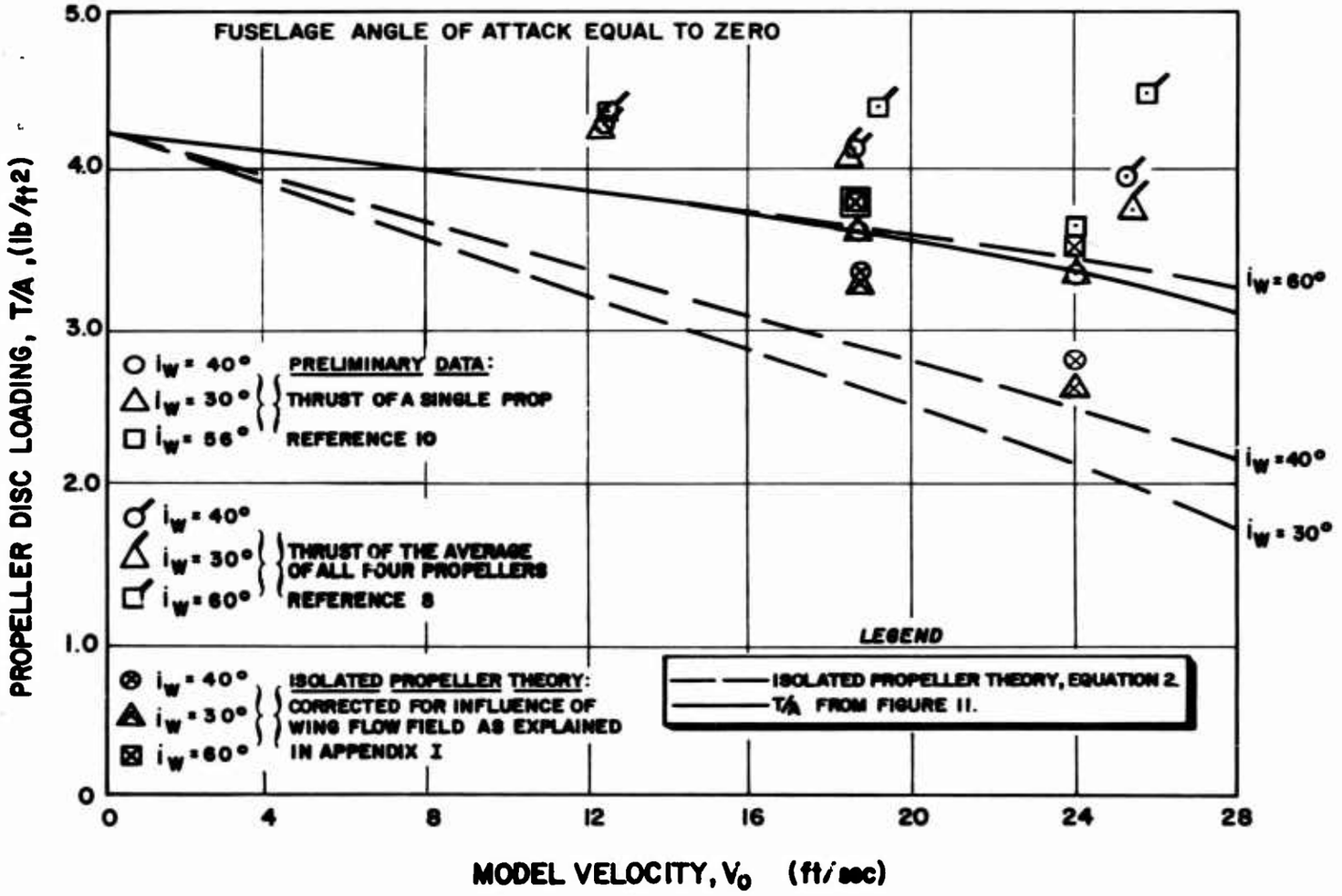

Figure 13. Theoretical Correction of Propeller Thrust for Wing Interference. Comparison With Experiment.

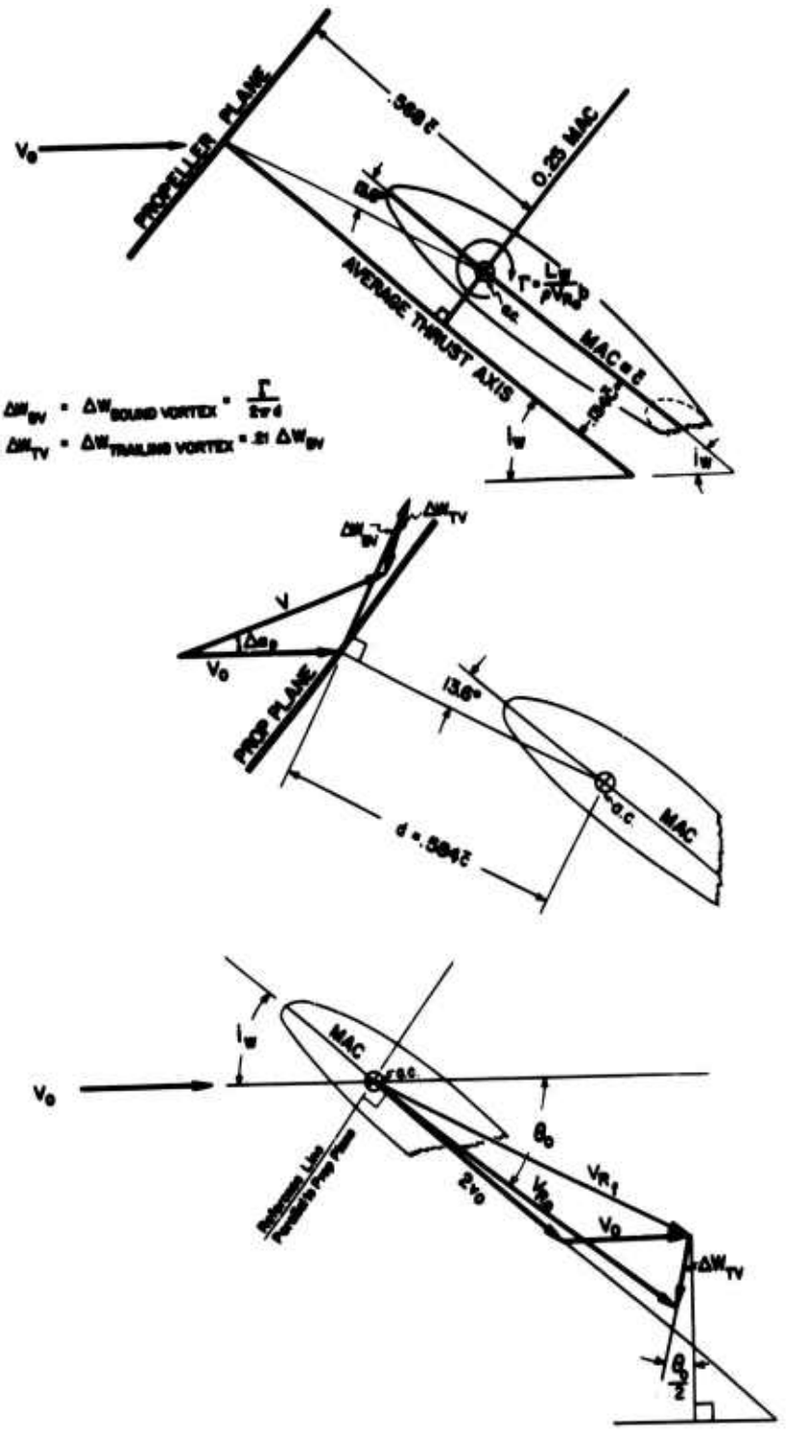

Figure 14. Diagram of Correction Applied to Flow Conditions at Propeller due to Wing Interference.

APPENDIX II
PREDICTION OF GROUND EFFECT

Reference 7 presents an analytical technique for estimating the flow conditions in the vicinity of an aircraft flying in proximity to a ground plane; the ground effect solution is a special case of a comprehensive treatment of wind tunnel wall effects. Then, if data are available on the aerodynamic characteristics of a vehicle out of ground effect, this theory may be used to calculate the effect of the presence of the ground on the aerodynamic forces acting on the vehicle by determining the changes in angle of attack and dynamic pressure at the model due to an image system. The approach taken in this reference is to replace the actual aircraft flow field by a line of singularities representing the aircraft's wake, the strength and position being determined by the experimentally determined momentum flow characteristics of the aircraft. An equal and opposite image wake system satisfying the boundary conditions at the ground plane is then used to replace the ground plane. Influence velocities, δu and δw, are then computed at the vehicle due to the presence of the image system.

Implementation of this theory is greatly aided by the use of charts such as the one shown in Figure 15 and adapted from Reference 7. This chart is a plot of nondimensional horizontal and vertical influence coefficients as functions of wake angle;* these coefficients, when multiplied by the proper momentum velocity and altitude ratio, give the two components of influence velocity at the model (δu and δw), as indicated on the figure.

In the following, the theory of Reference 7 is used to calculate theoretically the effect of the presence of the ground on the forces acting on the configuration of interest by applying corrections to the wing and propeller forces independently. The propeller thrust is corrected with the aid of the experimental data given in Figure 11, and the wing forces are altered by purely analytical means. This application should give some indication of how successful the application of ground effect corrections based on an analytical approach will be with respect to the aerodynamic characteristics of a tilt-wing aircraft. Only lift and drag are considered in the following discussion.

*For the computations, the wake angle, θ_n (the angle between the free-stream velocity and the line of singularities representing the wake), has been taken as one-half the value given by the momentum theory considerations of Reference 7. This is a result of treatment such as that of Reference 12, which shows that, for an elliptically loaded wing, the vortex system moves downward at an average velocity of approximately 0.4 times the momentum value of the remote downwash.

In the present application of this theory, it was noted that the influence velocities obtained were sufficiently large, compared to the free-stream velocity, to alter materially the wake angle predicted on the basis of out-of-ground-effect conditions. Accordingly, an iteration procedure was used to converge on a final wake deflection angle that included the presence of the influence velocities; convergence of the iteration was aided by the use of graphical procedures. Throughout this computation, it was assumed that the forces on the model did not change.

In the absence of comprehensive experimental data on the complete model forces as functions of velocity and angle of attack, it was necessary to use a partly analytical approach to apply ground effect corrections. The technique employed is shown by the velocity vector diagrams of Figures 16a through 22a, and the results are presented in Figures 16b through 22b as polar plots of the total and component forces in and out of ground effect. The correction procedure is as follows:

1. Construct a velocity vector polygon composed of:

   $2v_0$, the fully developed propeller induced velocity, as determined from Figure 11 and momentum theory.

   V_0, the free-stream velocity.

   Δw_{TV}, the wing induced velocity, due to a pair of trailing vortices (as in Appendix I), directed perpendicular to the wake angle found above.

   V_{R_0} is the resultant of these velocities. The bound vortex gives no contribution, since calculation is being made at the aerodynamic center of the wing.

2. Correct the propeller thrust for the effect of the ground effect influence velocities δu and δw by using the experimental data of Figure 11. Then compute a corrected propeller induced velocity $(2v_0 + \Delta v)$, using momentum theory.

3. Reconstruct the velocity polygon, including Δv, Δw_{TV}, δu, and δw, to determine a corrected vector resultant velocity, V_R.

4. Correct the wing force coefficients of Figures 16 through 22 by the relation

$$C_{W,S_{CORR}} = \left(\frac{V_R}{V_{R_0}}\right)^2 C_{W,S}$$

It should be noted that no correction of wing force for a change in local angle of attack has been attempted. A useful analytical model for determining the proper wing local angle of attack and lift curve slope is not part of the simple approach outlined above;[13] and since the angle between V_R and V_{R_O} is typically small, this effect was neglected.

The results of this procedure, shown in Figures 16b through 22 , indicate that for high wing incidence, the trend of ground effect on the forces is reasonably well predicted and the magnitudes are only slightly underpredicted; for the lowest wing incidence case ($i_W = 30°$), the magnitude is overpredicted. This difference may result from the fact that wing force changes due to angle of attack were not included. The change in angle of attack will become increasingly important at low wing incidence trim conditions where the wing lift curve slope approaches its power-off value and the vertical influence velocity effects tend to predominate (as in conventional ground effect conditions).

The foregoing procedure is a very simplified analysis that neglects all distributed effects such as the spanwise and chordwise distribution of wing vorticity and the distribution of induced flow at the wing and propeller. This simplified analysis is of value in that it predicts the important trends of the ground proximity effects and aids in the interpretation of the observed behavior of the aircraft and the experimental model data.

HORIZONTAL INFLUENCE VELOCITY

$$\delta u = \frac{A_m v_o}{4h^2}(\delta_{u,D} + \delta_{u,L})$$

VERTICAL INFLUENCE VELOCITY

$$\delta w = \frac{A_m v_o}{4h^2}(\delta_{w,D} + \delta_{w,L})$$

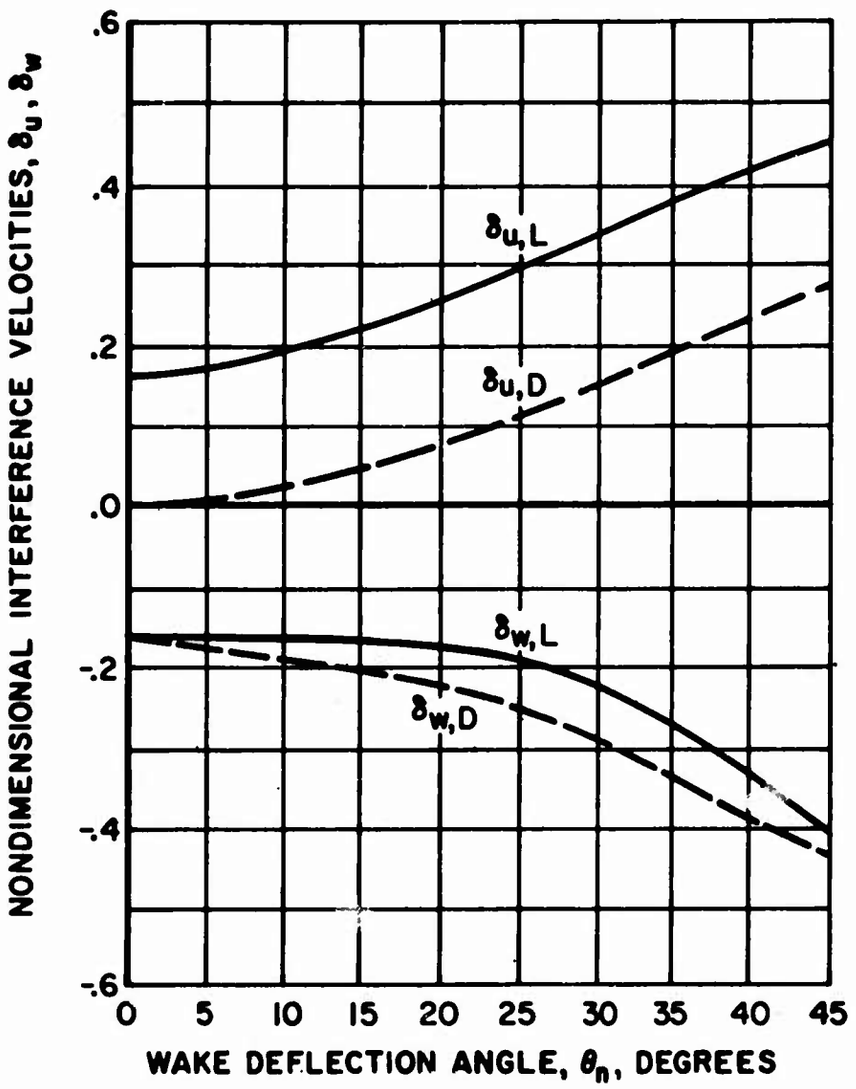

Figure 15. Ground Effect Influence Velocity Coefficients From Reference 7.

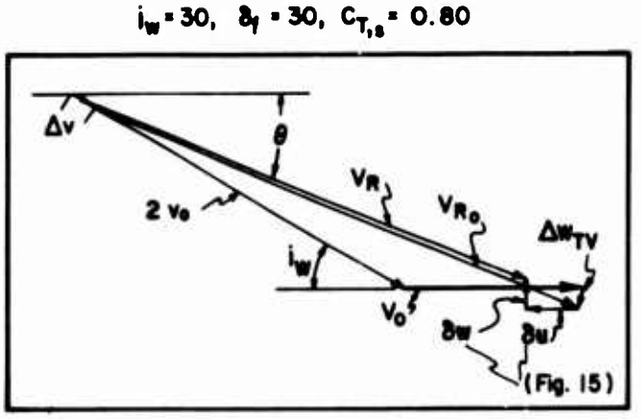

FIGURE 16a. DIAGRAM USED TO DETERMINE VELOCITY AT WING FOR CORRECTION OF WING FORCE DUE TO GROUND EFFECT.

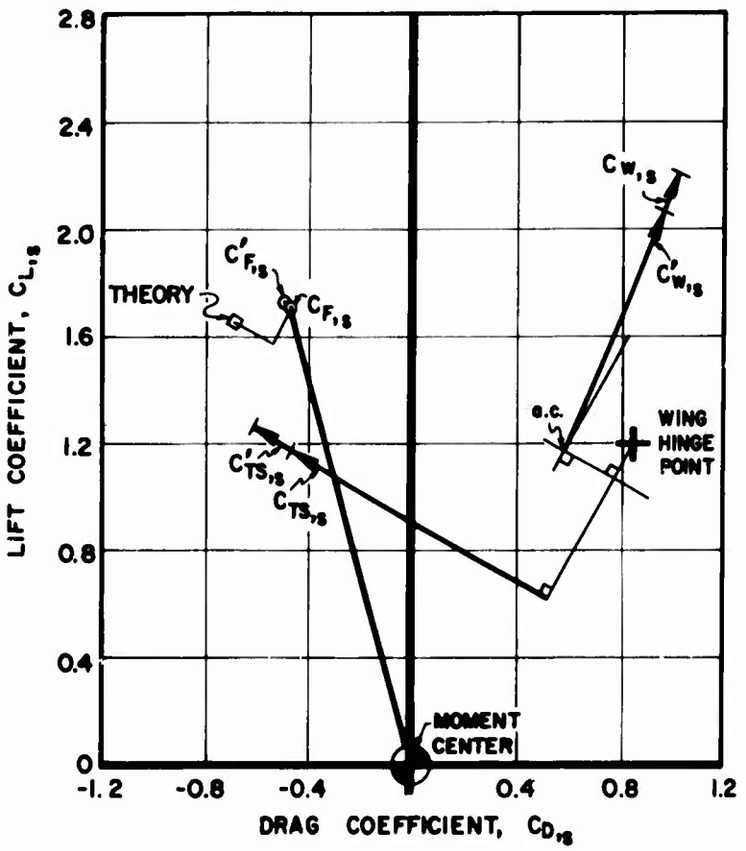

FIGURE 16b. THEORETICAL GROUND EFFECT ON MODEL FORCE COEFFICIENTS.

Figure 16. Theoretical Calculation of Ground Effect. ($i_w = 30°$, $\delta_f = 30°$, $C_{T,s} = 0.80$)

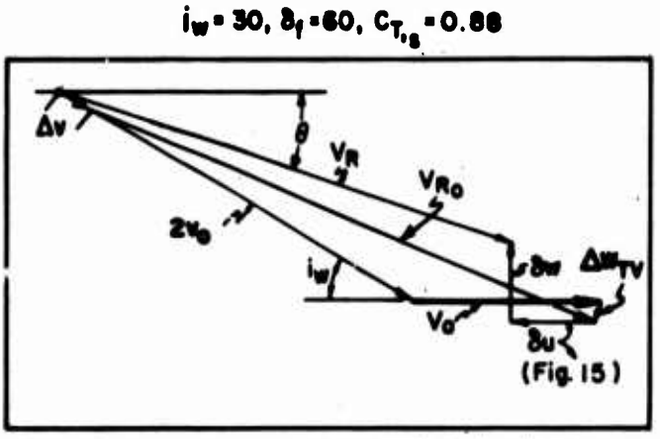

FIGURE 17a. DIAGRAM USED TO DETERMINE VELOCITY AT WING FOR CORRECTION OF WING FORCE DUE TO GROUND EFFECT.

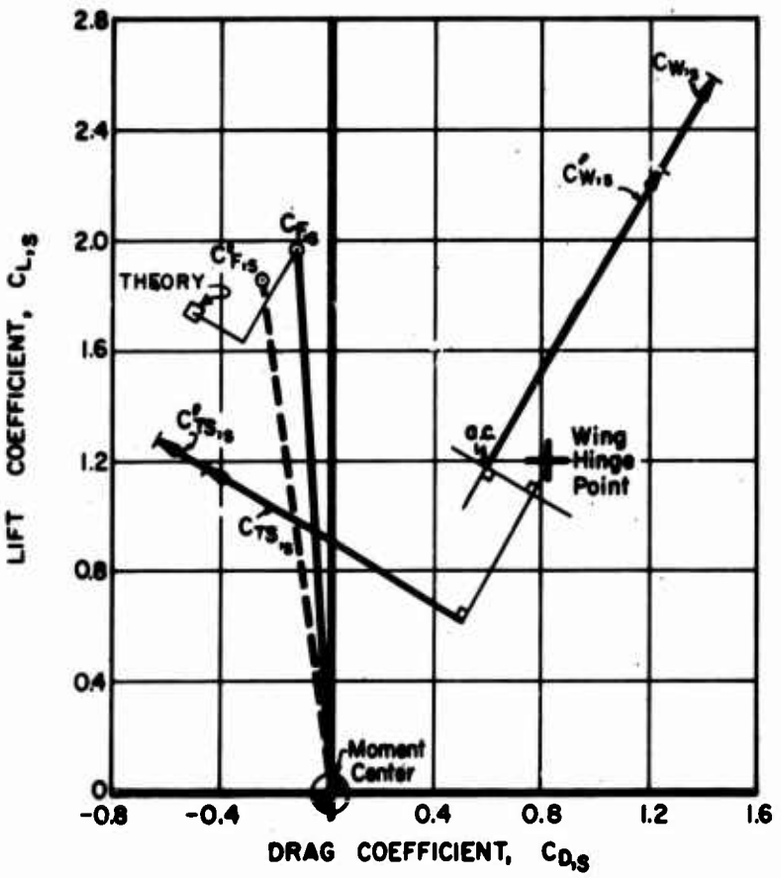

FIGURE 17b. THEORETICAL GROUND EFFECT ON MODEL FORCE COEFFICIENTS.

Figure 17. Theoretical Calculation of Ground Effect. ($i_w = 30°$, $\delta_f = 60°$, $C_{T,s} = 0.88$)

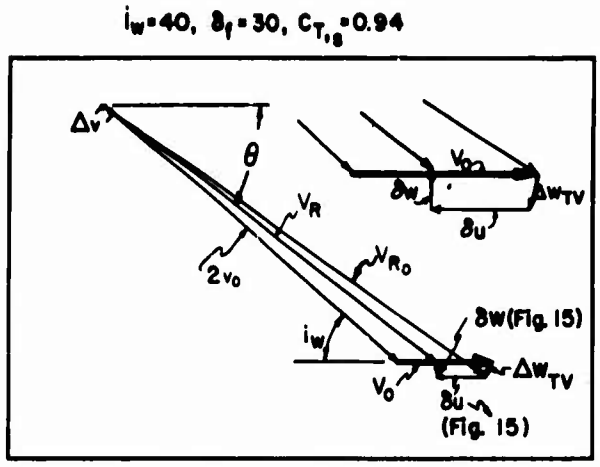

FIGURE 18a. DIAGRAM USED TO DETERMINE VELOCITY AT WING FOR CORRECTION OF WING FORCE DUE TO GROUND EFFECT.

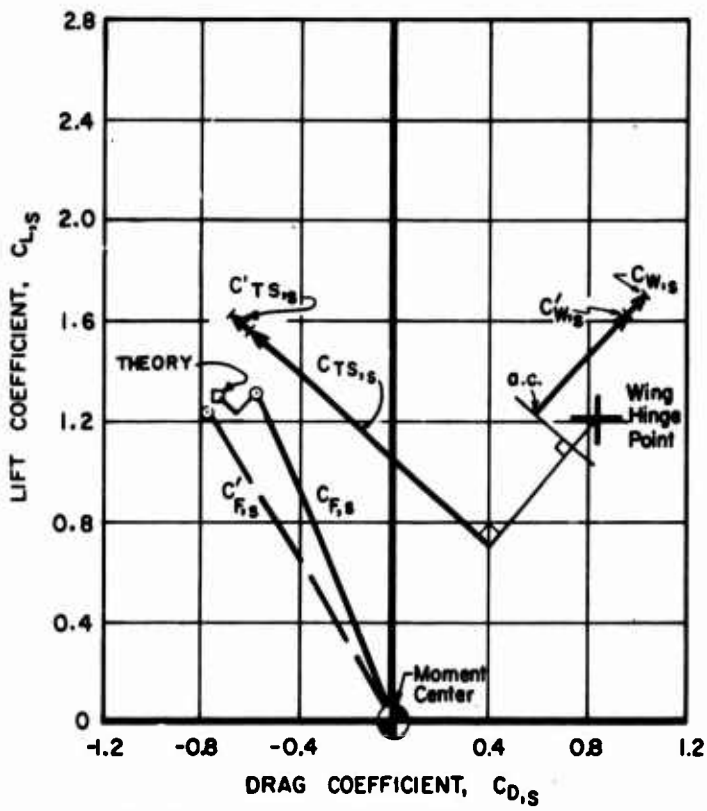

FIGURE 18b. THEORETICAL GROUND EFFECT ON MODEL FORCE COEFFICIENTS.

Figure 18. Theoretical Calculation of Ground Effect. ($i_w = 40°$, $\delta_f = 30°$, $C_{T,_s} = 0.94$)

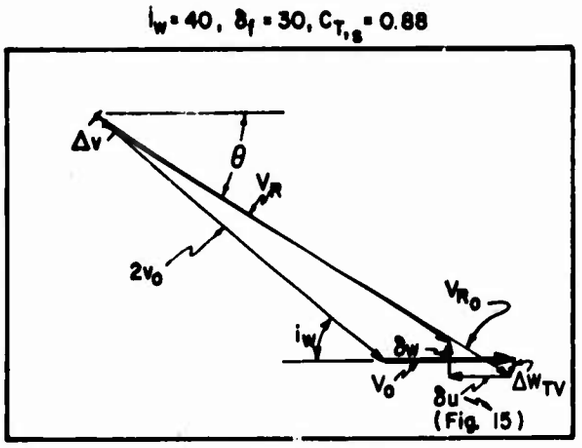

FIGURE 19a. DIAGRAM USED TO DETERMINE VELOCITY AT WING FOR CORRECTION OF WING FORCE DUE TO GROUND EFFECT.

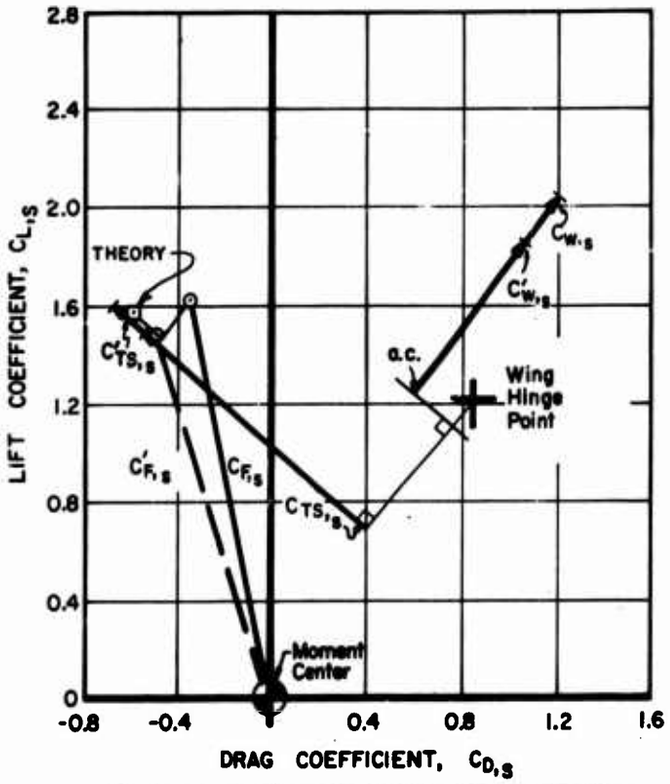

FIGURE 19b. THEORETICAL GROUND EFFECT ON MODEL FORCE COEFFICIENTS.

Figure 19. Theoretical Calculation of Ground Effect. ($i_w = 40°$, $\delta_f = 30°$, $C_{T,s} = 0.88$)

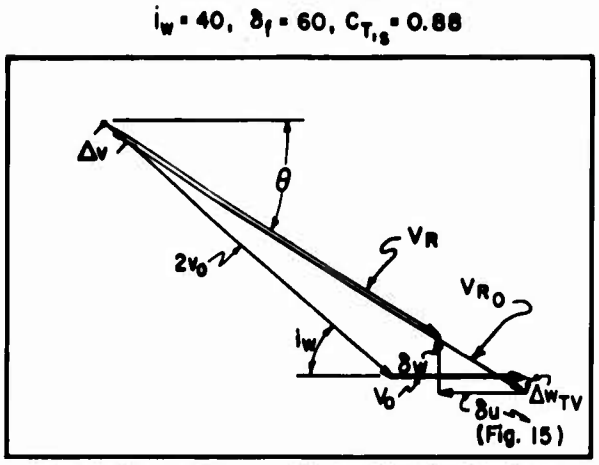

FIGURE 20a. DIAGRAM USED TO DETERMINE VELOCITY AT WING FOR CORRECTION OF WING FORCE DUE TO GROUND EFFECT.

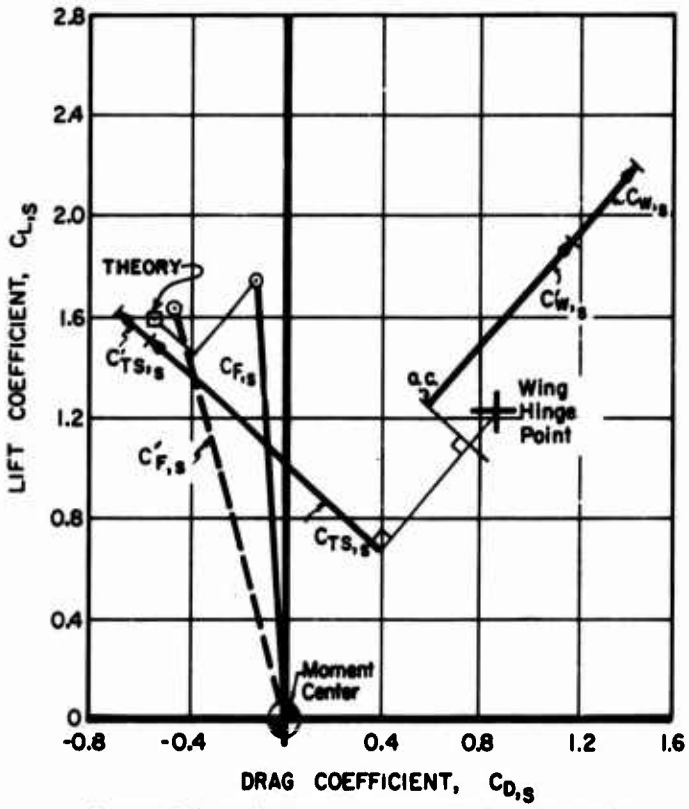

FIGURE 20b. THEORETICAL GROUND EFFECT ON MODEL FORCE COEFFICIENTS

Figure 20. Theoretical Calculation of Ground Effect. ($i_w = 40°$, $\delta_f = 60°$, $C_{T,s} = 0.88$)

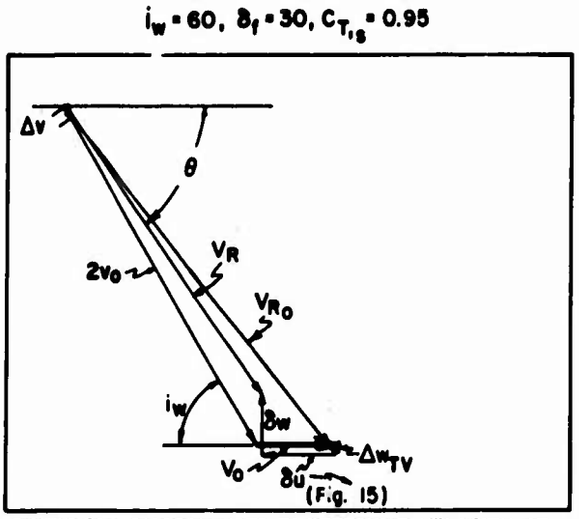

FIGURE 21 a. DIAGRAM USED TO DETERMINE VELOCITY AT WING FOR CORRECTION OF WING FORCE DUE TO GROUND EFFECT

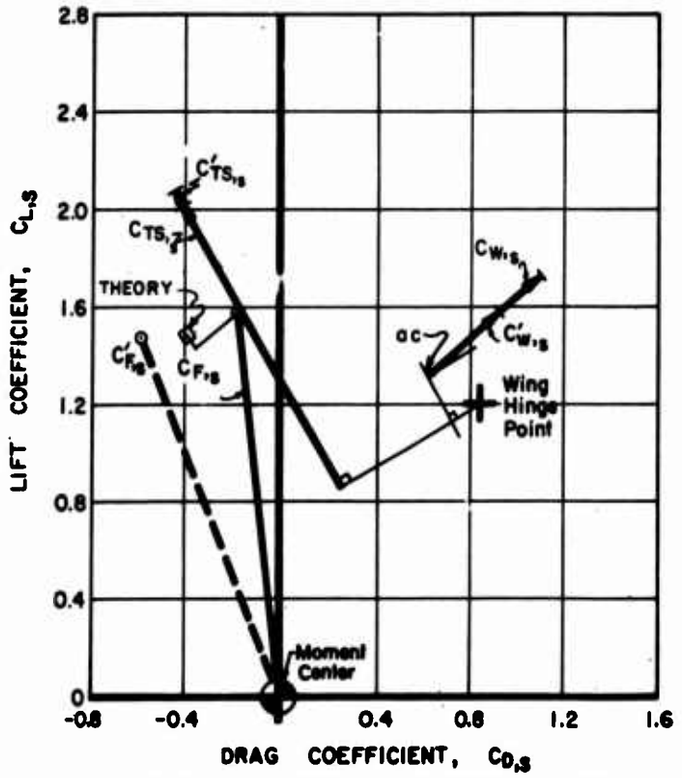

FIGURE 21 b.- THEORETICAL GROUND EFFECT ON MODEL FORCE COEFFICIENTS.

Figure 21. Theoretical Calculation of Ground Effect. ($i_w = 60°$, $\delta_f = 30°$, $C_{T,s} = 0.95$)

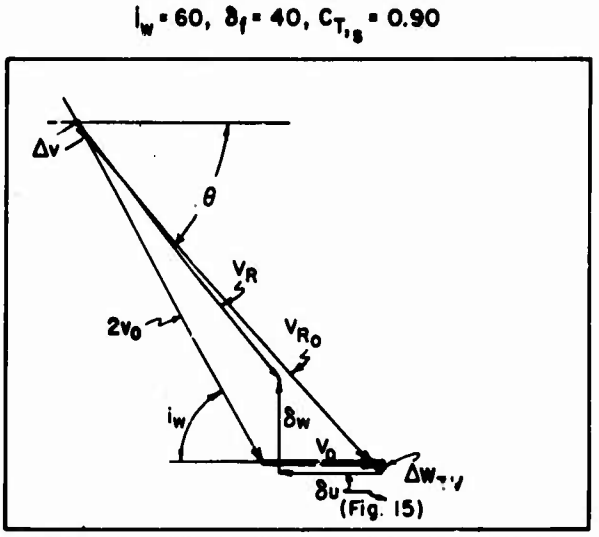

FIGURE 22 a. DIAGRAM USED TO DETERMINE VELOCITY AT WING FOR CORRECTION OF WING FORCE DUE TO GROUND EFFECT

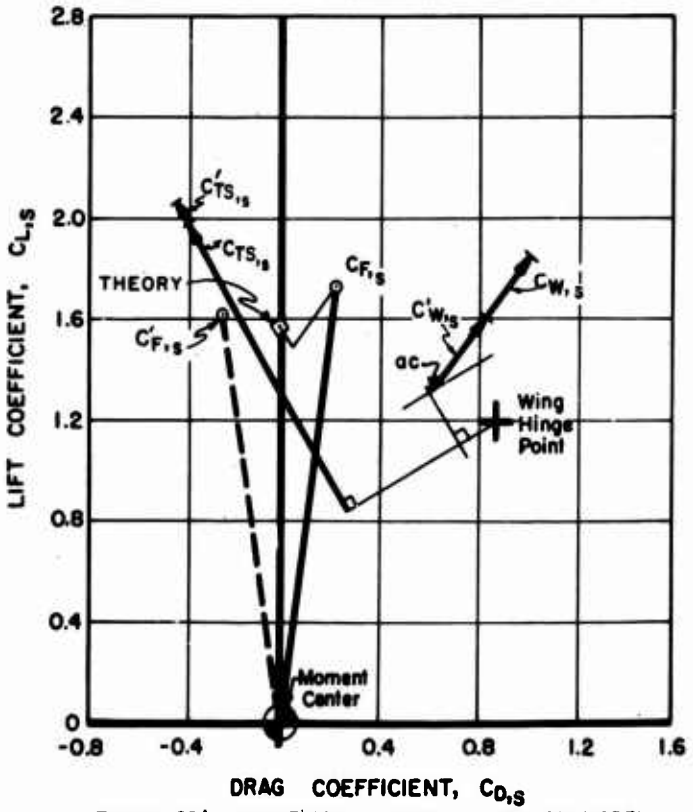

FIGURE 22 b. THEORETICAL GROUND EFFECT ON MODEL FORCE COEFFICIENTS

Figure 22. Theoretical Calculation of Ground Effect. ($i_w = 60°$, $\delta_f = 40°$, $C_{T,_s} = 0.90$)

Unclassified

Security Classification

DOCUMENT CONTROL DATA - R&D

(Security classification of title, body of abstract and indexing annotation must be entered when the overall report is classified)

1. ORIGINATING ACTIVITY (Corporate author)

Department of Aerospace and Mechanical Sciences
Princeton University

2a. REPORT SECURITY CLASSIFICATION

Unclassified

2b. GROUP

-

3. REPORT TITLE

An Experimental Investigation of Ground Effect on a Four-Propeller Tilt-Wing V/STOL Model

4. DESCRIPTIVE NOTES (Type of report and inclusive dates)

Final Technical Report

5. AUTHOR(S) (Last name, first name, initial)

William F. Putman

6. REPORT DATE	7a. TOTAL NO. OF PAGES	7b. NO. OF REFS
July 1968	65	14

8a. CONTRACT OR GRANT NO.	9a. ORIGINATOR'S REPORT NUMBER(S)
DA 44-177-AMC-8(T) b. PROJECT NO. 1F125901A14233 c. d.	USAAVLABS Technical Report 68-45 9b. OTHER REPORT NO(S) (Any other numbers that may be assigned this report) Princeton Univ. Aero. & Mech. Sci. Report No. 892

10. AVAILABILITY/LIMITATION NOTICES

This document has been approved for public release and sale; its distribution is unlimited.

11. SUPPLEMENTARY NOTES	12. SPONSORING MILITARY ACTIVITY
-	U.S. Army Aviation Materiel Laboratories Fort Eustis, Virginia

13. ABSTRACT

Tests were conducted on a one-tenth scale model of a tilt-wing V/STOL at specified points simulating flight conditions at various heights above the ground. The model was moved at selected velocities through still air in the Princeton Track; and lift, drag, and pitching moment were measured at various heights above the ground.

Investigations included combinations of 30°, 40°, and 60° wing incidence angle with 30°, 40°, and 60° flap deflection, and thrust coefficients ranging from 0.80 to 0.95. Model ground clearances of 3.5 to 36 inches were investigated both at constant altitude and with the altitude continuously varying during the run.

The data are presented as plots of lift, drag, and pitching moment coefficients. Also included are data from wind tunnel tests on similar models.

A brief analysis is made of ground effect phenomena and an understanding of the general data trends is obtained. The magnitude and direction of the force change in ground effect are predictable. However, the pitching moment change is strongly influenced by factors such as the flow field beneath the fuselage, the change in downwash at the horizontal tail, and other effects.

DD FORM 1 JAN 64 1473

Unclassified

Security Classification

Unclassified

Security Classification

14. KEY WORDS	LINK A		LINK B		LINK C	
	ROLE	WT	ROLE	WT	ROLE	WT
Airplanes, VTOL Airplanes, Tilt-Wing Ground Effect						

INSTRUCTIONS

1. **ORIGINATING ACTIVITY:** Enter the name and address of the contractor, subcontractor, grantee, Department of Defense activity or other organization *(corporate author)* issuing the report.

2a. **REPORT SECURITY CLASSIFICATION:** Enter the overall security classification of the report. Indicate whether "Restricted Data" is included. Marking is to be in accordance with appropriate security regulations.

2b. **GROUP:** Automatic downgrading is specified in DoD Directive 5200.10 and Armed Forces Industrial Manual. Enter the group number. Also, when applicable, show that optional markings have been used for Group 3 and Group 4 as authorized.

3. **REPORT TITLE:** Enter the complete report title in all capital letters. Titles in all cases should be unclassified. If a meaningful title cannot be selected without classification, show title classification in all capitals in parenthesis immediately following the title.

4. **DESCRIPTIVE NOTES:** If appropriate, enter the type of report, e.g., interim, progress, summary, annual, or final. Give the inclusive dates when a specific reporting period is covered.

5. **AUTHOR(S):** Enter the name(s) of author(s) as shown on or in the report. Enter last name, first name, middle initial. If military, show rank and branch of service. The name of the principal author is an absolute minimum requirement.

6. **REPORT DATE:** Enter the date of the report as day, month, year, or month, year. If more than one date appears on the report, use date of publication.

7a. **TOTAL NUMBER OF PAGES:** The total page count should follow normal pagination procedures, i.e., enter the number of pages containing information.

7b. **NUMBER OF REFERENCES:** Enter the total number of references cited in the report.

8a. **CONTRACT OR GRANT NUMBER:** If appropriate, enter the applicable number of the contract or grant under which the report was written.

8b, 8c, & 8d. **PROJECT NUMBER:** Enter the appropriate military department identification, such as project number, subproject number, system numbers, task number, etc.

9a. **ORIGINATOR'S REPORT NUMBER(S):** Enter the official report number by which the document will be identified and controlled by the originating activity. This number must be unique to this report.

9b. **OTHER REPORT NUMBER(S):** If the report has been assigned any other report numbers *(either by the originator or by the sponsor)*, also enter this number(s).

10. **AVAILABILITY/LIMITATION NOTICES:** Enter any limitations on further dissemination of the report, other than those imposed by security classification, using standard statements such as:

(1) "Qualified requesters may obtain copies of this report from DDC."

(2) "Foreign announcement and dissemination of this report by DDC is not authorized."

(3) "U. S. Government agencies may obtain copies of this report directly from DDC. Other qualified DDC users shall request through _____."

(4) "U. S. military agencies may obtain copies of this report directly from DDC. Other qualified users shall request through _____."

(5) "All distribution of this report is controlled. Qualified DDC users shall request through _____."

If the report has been furnished to the Office of Technical Services, Department of Commerce, for sale to the public, indicate this fact and enter the price, if known.

11. **SUPPLEMENTARY NOTES:** Use for additional explanatory notes.

12. **SPONSORING MILITARY ACTIVITY:** Enter the name of the departmental project office or laboratory sponsoring *(paying for)* the research and development. Include address.

13. **ABSTRACT:** Enter an abstract giving a brief and factual summary of the document indicative of the report, even though it may also appear elsewhere in the body of the technical report. If additional space is required, a continuation sheet shall be attached.

It is highly desirable that the abstract of classified reports be unclassified. Each paragraph of the abstract shall end with an indication of the military security classification of the information in the paragraph, represented as *(TS), (S), (C), or (U)*.

There is no limitation on the length of the abstract. However, the suggested length is from 150 to 225 words.

14. **KEY WORDS:** Key words are technically meaningful terms or short phrases that characterize a report and may be used as index entries for cataloging the report. Key words must be selected so that no security classification is required. Identifiers, such as equipment model designation, trade name, military project code name, geographic location, may be used as key words but will be followed by an indication of technical context. The assignment of links, rules, and weights is optional.

GPO 886-551

Unclassified

Security Classification